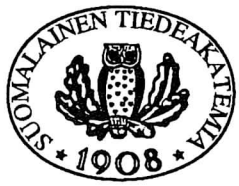


THE FINNISH ACADEMY OF SCIENCE AND LETTERS
SODANKYLÄ GEOPHYSICAL OBSERVATORY

# HIGH LATITUDE D-REGION STUDIES BY INCOHERENT SCATTER RADAR MEASUREMENTS

**Esa Turunen**

Academic Dissertation to be presented with the assent of the Faculty of Science, University of Oulu, Finland, for public discussion in the Municipal Hall, Sodankylä, Finland, on April 17th, 1993, at 12 o'clock noon.

Sodankylä Geophysical Observatory
Sodankylä, Finland

Report No. 52
April 1993

ISBN 952-9811-00-4
ISSN 0359-3657

University of Oulu
Printing Center
Oulu 1993

**Turunen, Esa,** High latitude D-region studies by incoherent scatter radar measurements
The Finnish Academy of Science and Letters
Sodankylä Geophysical Observatory, Sodankylä, Finland
Report No. 52, April 1993

*Abstract*

This thesis develops the interpretation of incoherent scatter radar measurements at the ionospheric D-region altitudes through a series of six original papers. Properties of the high latitude D-region are deduced from the power, Doppler shift and spectral width of the scattered signal, as measured by the European Incoherent Scatter Radar facility (EISCAT) located in Ramfjordmoen, near Tromsø, Norway. Data correction methods are developed and applied to get reliable estimates of the electron density, the neutral wind velocity, the ion-neutral collision frequency, the temperature, the mean ion mass and the negative ion to electron concentration ratio in D-region. A new method of data interpretation is presented. The mathematical solution of a detailed ion-chemistry model, appropriate for D-region, is coupled to the application of the traditional incoherent scatter theory.

Keywords: incoherent scatter, D-region, ion chemistry

*To my dear wife Raili,*

*my sons Johannes and Sampo*

*and my yet unnamed daughter*

*Acknowledgements*

I thank the Geophysical Observatory of the Finnish Academy of Science and Letters for giving me the opportunity to carry out this work. I wish to express my sincere thanks to my thesis advisor, Dr. Tauno Turunen, whose scientific attitude to a problem of any kind has taught me to enjoy even the lonely nights spent when writing this. I am also greatly indebted to Mrs. Mirja Hämäläinen for her patience in typing the $n^{th}$ version of many parts of the manuscripts. Special thanks are due to Päiviö Pollari and Helena Matveinen for assistance in calculations. I would like to thank all the personnel of the Geophysical Observatory and the EISCAT Sodankylä site for continuous encouragement, especially Jussi Markkanen and Johannes Kultima for many endless discussions about the philosophy of measurements and Dr. Hilkka Ranta for introducing me to the world of cosmic radio noise absorption. Finally, I wish to thank my beloved parents who initially made this work possible.

## List of original papers


[1] HARGREAVES J.K., H. RANTA, A. RANTA, E. TURUNEN, T. TURUNEN
Observations of the polar cap absorption event of February 1984 by the EISCAT incoherent scatter radar, Planet. Space Sci., 35, 947-958, 1987.

[2] POLLARI P., A. HUUSKONEN, E. TURUNEN, T.TURUNEN
Range ambiguity effects in a phase coded D-region incoherent scatter radar experiment, J. Atmos. Terr. Phys., 51, 11/12, 937-945, 1989.

[3] TURUNEN E., P.N. COLLIS, T. TURUNEN
Incoherent scatter spectral measurements of the summertime high-latitude D-region with the EISCAT UHF radar, J. Atmos. Terr. Phys., 50, 289-299, 1988.

[4] HANSEN G., U-P. HOPPE, E. TURUNEN, P. POLLARI
Comparison of observed and calculated incoherent scatter spectra from the D region. Radio Science, 26, 5, 1153-1164, 1991.

[5] BURNS C.J., E. TURUNEN, H. MATVEINEN, H. RANTA, J.K. HARGREAVES
Chemical modelling of the quiet summer D- and E-regions using EISCAT electron density profiles, J. Atmos. Terr. Phys., 53, 1/2, 115-134, 1991.

[6] TURUNEN E.
EISCAT incoherent scatter radar observations and model studies of day to twilight variations in the D-region during the PCA event of August 1989, J. Atmos. Terr. Phys., 55, 4/5, 767-781, 1993.


The original papers are referred in the text by their numbers in brackets.

CONTENTS

# 1. INTRODUCTION

It is a fascinating opportunity to be able to monitor the near earth environment by a ground based remote sensing instrument, which is not only performing continuous measurement, but also capable of providing information about several aeronomical parameters of interest, all at the same time. While many different radio techniques are available for this purpose, only incoherent scatter radars have been used to estimate such a wide range of parameters as electron concentration, plasma velocity, neutral wind velocity, electric field and currents, electron, ion and neutral temperatures, ion mass, ion composition, ion-neutral collision frequency, neutral density, Hall and Pedersen conductivity, energy deposition of precipitating electrons, their energy spectrum and Joule energy deposition, just to mention a few. Many other parameters can be derived from these as a combination, or by using additional assumptions.

The first incoherent scatter measurements of D-region electron density were made by LaLonde (1966) in Arecibo, Puerto Rico. Altitude resolution was 3–6 km and the minimum observable electron density around 1000 electrons per cubic centimeter. Early electron density measurements elsewhere were reported by Armistead et al. (1972) at Millstone Hill, USA and by Taylor (1975) at Malvern, UK. D-region measurements at Jicamarca, Peru, were shown to be dominated by turbulent scatter (Rastogi and Woodman, 1974). The early electron density measurements are reviewed by Sechrist (1974). As the experimental technique was developed, Mathews et al. (1982) found a minimum detectable electron density of 100 electrons per cubic centimeter. Results from the first spectral measurements using pulse-to-pulse correlation methods were given by Mathews (1976) and Harper (1978). Since then, extensive work was done in Arecibo to determine aeronomical parameters including winds, temperature, pressure, negative ion and positive ion concentrations and to some extent also ion mass. These results are reviewed by Mathews (1981, 1984).

At the European Incoherent Scatter Facility EISCAT (Folkestad et al., 1983), the first mesospheric spectra were obtained in 1982 by Kofman et al. (1984). The data however suffered from inaccuracies and the authors were cautious to interpret their results. Later development (Turunen, 1986) of the experimental technique for D-region lead, e.g., to results presented in this thesis. The D-region research by the EISCAT radars is reviewed by Collis and Röttger (1990). A recent review including also Arecibo results is given by Hall (1990). A major research effort has been initiated by EISCAT measurements since the detection of unexpectedly strong radar backscatter by the EISCAT VHF radar (Hoppe et al., 1988), at narrow altitude regions near mesopause in summer. Investigations of these Polar Mesosphere Summer Echoes (PMSE, Röttger et al. 1988) also put forward further experimental development (see La Hoz et al., 1989), applying complementary codes and the ultimate altitude resolution of 150 m.

The ionospheric D-region is a challenging target for any measurement. The ionisation degree is low. Typical electron concentrations at the altitude of 70 km are of the order of 100 electrons per cubic centimeter. In these few electrons, or actually, in the plasma properties due to the existence of these few electrons, lies our possibility to extract information on various physical parameters via probing by radiowaves. The incoherent scatter signal, resulting due to Thomson scattering from electrons

in the presence of plasma density fluctuations caused by ion acoustic waves, is much weaker than the signal from Fresnel scattering due to gradients transverse to radiowave propagation, or Bragg scattering due to irregularities caused by neutral air turbulence, which are observed with the MF- HF- and lower frequency VHF- radars. The occurence of the PMSE phenomenon at high latitudes additionally complicates the use of incoherent scatter technique, since the signal due to PMSE may totally dominate the measured data. Moreover, PMSE events, although being rare, were also shown to occur with the UHF radar (Röttger et al., 1990). The origin of PMSE is still somewhat unclear but definitely it is not caused by the incoherent scatter process. This was ruled out as a possible scattering mechanism already in the first investigations by Hoppe et al. (1988).

The chemistry of the D-region is complex. Transport phenomena affect the concentrations of long-lived constituents. Dynamics plays a key role. Tens of important neutral and ionic constituents form a system whose response to forcing from above and below is difficult to model exactly. This forcing includes processes like heat conduction from the region above, heat loss by infrared radiation, adiabatic heating and cooling, momentum and heat deposition by dissipating tides, planetary waves and gravity waves, and direct effects on composition by particle precipitation events and solar radiation variations. Any calculation of the energy balance should also include estimation of the energy input in the region above, which is characterized by absorption of solar EUV and UV radiation, Joule dissipation of ionospheric currents, dissipation of wave and turbulent energy, and particle precipitation. The appearance of aerosol particles, ice and dust, their possible charging and the interplay of aeronomy and dynamics, as manifested, e.g., by the PMSE phenomenon, challenge any realistic modelling effort of the mesopause region.

A drawback of the incoherent scatter radar, as a routine instrument in investigations of ionospheric D-region, is that sophisticated installations and experiments are needed because of the properties of the target region. To overcome the difficulties with weak signals, one needs to introduce transmitter power in megawatt class, and antenna sizes like 305 meters in diameter for the Arecibo radar in Puerto Rico, or 40 times 120 meters in area for the EISCAT VHF radar in Tromsø. Fortunately, at high latitudes excess ionisation in D-region often occurs as a consequence of the precipitation of high energy electrons, or during solar proton events. Thus the EISCAT UHF radar, with its antenna dish of only 32 meters, also appears as a practical tool for investigating the D-region, as is shown in this thesis. Unfortunately, it turns out that the incoherent scatter signal from the D-region contains the effect of several physical parameters in one measured parameter, the spectral width. One is usually thus obliged to use neutral atmospheric models, independent measurements, or a priori assumptions on the behaviour of the physical system, if any of the unknown physical variables is to be determined. This is in contrast to the situation in E- and F-regions, where different parameters have different effects on the measured spectral form.

This thesis develops the interpretation of incoherent scatter radar measurements at the ionospheric D-region altitudes through a series of six original papers. Properties of the high latitude D-region are deduced from the power, Doppler shift and spectral width of the scattered signal, as measured by the European Incoherent Scatter Radar facility, EISCAT. Section 2 reviews the incoherent scatter theory which describes Thomson scattering from a weakly ionised, collisional multicomponent plasma. It is shown that the formulation by Fukuyama and Kofman (1980), with a mean ion mass description, is in excellent agreement with the full description obtained following Dougherty and Farley (1960,1963) and Swartz and Farley (1979). Comparison is presented for the case where 36 different plasma components are considered. Section 3 presents a description of the D-region in the form of an

ion chemistry model. The model was used in papers [5] and [6]. Section 3 is intended to give a self-contained description of the model.

Section 4 describes experiment-specific correction methods which are applied to get reliable estimates of the electron density, the neutral wind velocity, the ion-neutral collision frequency, neutral nitric oxide concentration, the mean ion mass, the negative ion to electron concentration ratio and the temperature in D-region, using the theory presented in section 2 and the model of section 3. A new method of data interpretation is presented. The mathematical solution of the detailed ion chemistry model is coupled to the application of the traditional incoherent scatter theory. Thus several aeronomical parameters of interest are extracted simultaneously from the measured incoherent scatter data. Results obtained in the original papers are reviewed in section 5 and conclusions based on the results are summarized in section 6.

## 2. INCOHERENT SCATTER FROM COLLISIONAL PLASMA

Let us denote the incident angular frequency of the transmitted radar signal by $\omega_o$ and the Doppler shift from this frequency due to incoherent scatter by $\omega$. Further, in the following the contributions from all ions are subscripted by $I$, from a single ion species by $i$, and from electrons by $e$. Following the formulation given by Dougherty and Farley (1960, 1963) and Swartz and Farley (1979), the incoherent scatter power spectrum $\sigma$ is given by the expression:

$$\sigma(\omega+\omega_o)d\omega = \frac{N_e r_e^2}{\pi\omega}\left[\frac{|Y_e|^2 Re(Y_I) + |\mu Y_I + i\lambda_D^2 k^2|^2 Re(Y_e)}{|Y_e + \mu Y_I + i\lambda_D^2 k^2|^2}\right] d\omega \quad , \tag{1}$$

where

$r_e$ = classical electron radius ,

$\lambda_D$ = electron Debye length ,

$$\mu = \frac{T_e}{T_i} \quad ,$$

$T_s$ = temperature of species s ,

$$Y_I = \sum_{s=ions} \eta_s Y_s \qquad \text{complex admittance function ,}$$

$$\eta_s = \frac{N_s q_s^2}{N_e e^2} \quad ,$$

$N_s$ = concentration of species s ,

$q_s$ = charge of species s ,

$e$ = charge of electron ,

$$Y_s = \frac{i + (\theta_s - i\Psi_s) J_s(\theta_s - i\Psi_s, \phi_s, \gamma)}{1 - \Psi_s J_s(\theta_s - i\Psi_s, \phi_s, \gamma)} \quad ,$$

$$\theta_s = \frac{\omega}{\sqrt{2} k v_s} \qquad \text{normalized frequency ,}$$

$$v_s = \sqrt{\frac{k_B T_s}{m_s}} \qquad \text{thermal velocity of species s ,}$$

$k_B$ = Boltzmann constant ,

$m_s$ = mass of species s ,

$$\phi_s = \frac{\Omega_s}{\sqrt{2}kv_s} \qquad \text{normalized gyrofrequency ,}$$

$$\Omega_s = \frac{q_s B}{m_s c} \quad ,$$

$c$ = speed of light ,

$$\Psi_s = \frac{\nu_{sn}}{\sqrt{2}kv_s} \qquad \text{normalized species-neutral collision frequency ,}$$

$\nu_{sn}$ = species-neutral collision frequency ,

$\gamma$ = angle between wave vector $k$ and geomagnetic field $B$ ,

$$Y_e = \frac{i + (\frac{\theta_e}{\cos\gamma} - i\frac{\Psi_e}{\cos\gamma}) J_e(\frac{\theta_e}{\cos\gamma} - i\frac{\Psi_e}{\cos\gamma}, \phi_e, \gamma)}{1 - \Psi_s J_s(\theta_s - i\Psi_s, \phi_s, \gamma)} \quad ,$$

$$J_s(\theta_s - i\Psi_s, \phi_s, \gamma) = \int_0^\infty e^{-i(\theta_s - i\Psi_s)t - \frac{1}{\phi_s^2}\sin^2\gamma \sin^2(\frac{\phi_s}{2}t) - \frac{1}{4}t^2\cos^2\gamma} dt \qquad \text{, Gordeyev integral}$$

and

$$J_s = -iZ(-\theta_s + i\Psi_s) \quad ,$$

where Z is the plasma dispersion function.

In the collision dominated situation, appropriate for the D-region, the resulting spectrum can be divided into a narrower ion line component and a broader electron line component. The ion component has a Lorentzian form and can thus be described by two parameters, the amplitude at zero Doppler shift and the spectrum width at half amplitude. In practice, the measured spectra have also additional contributions appearing as a constant Doppler shift due to the bulk drift velocity and a baseline shift due to noise and instrumental effects. One should note that an apparent baseline will appear also due to the frequency aliasing effect, if the bandwith of the experiment is limited.

Incoherent scatter from a three component plasma, consisting of positive ions, negative ions and electrons, was considered by Mathews (1978) and Fukuyama and Kofman (1980). If the electron temperature and ion temperature are assumed to be equal, expression (1) can be integrated analytically (Tanenbaum, 1968; Mathews, 1978) to give the total power in the spectrum. This is seen to be directly proportional to electron density in the first approximation. A raw electron density estimate $N_e^{raw}$ can be written in the form of the radar equation as

$$N_e^{raw} = C_{sys} \frac{k_B T_{cal} b r^2}{P_t \tau} \frac{P_{rec}}{P_{cal} - P_{bac}} \quad , \tag{2}$$

where

$C_{sys}$ = radar system constant ,

$T_{cal}$ = calibration temperature ,

$b$ = filter bandwidth ,

$r$ = distance from the radar to the scattering volume ,

$P_t$ = transmitted power ,

$\tau$ = pulse length ,

$P_{rec}$ = received power ,

$P_{cal}$ = calibration power ,

and

$P_{bac}$ = background power .

The radar system constant contains all instrument specific gain factors, and a factor due to the scattering cross section of a single electron.

Fukuyama and Kofman (1980) developed both the kinetic approach, as Dougherty and Farley (1963) and the hydrodynamic approach, as Tanenbaum (1968), to compute mesospheric incoherent scatter spectra. Good consistency was found between the two approaches. From the ion line component of the incoherent scatter spectrum, one obtains expressions for electron density $N_e$ and the incoherent scatter spectral width, $\Delta\omega$, in the form

$$N_e^{raw} = \frac{2N_e(1+2\lambda)}{\left[2(1+\lambda) + \left(\frac{4\pi 69\sqrt{T}}{\lambda_r \sqrt{N_e}}\right)^2\right]\left[1 + \left(\frac{4\pi 69\sqrt{T}}{\lambda_r \sqrt{N_e}}\right)^2\right]} \tag{3}$$

and

$$\Delta\omega = \frac{32\pi^2 k_B}{\lambda_r^2} \frac{T}{m_i \nu_{in}} \frac{\left[2(1+\lambda) + \left(\frac{4\pi 69\sqrt{T}}{\lambda_r \sqrt{N_e}}\right)^2\right]}{\left[1 + \left(\frac{4\pi 69\sqrt{T}}{\lambda_r \sqrt{N_e}}\right)^2\right]} \quad , \tag{4}$$

where

$\lambda$ = negative ion to electron concentration ratio ,

$T$ = temperature ,

and

$\lambda_r$ = radar wavelength .

In deriving expression (4), the product of the ion mass and the ion-neutral collision frequency is assumed to be equal for the negative and positive ions. Expression (4) in somewhat different forms has been used in several investigations (see e.g. Fukuyama, 1981; Kofman et al., 1984; Ganguly, 1985; Fukyama et al., 1987; Kelley et al., 1987; Turunen et al., 1987; Hall et al., 1987; Collis et al., 1988; Hall and Brekke, 1988; Hall et al., 1988; Hoppe and Hansen, 1988; papers [2], [3], [4] and [6]). However, one might wonder how accurate this description is in a real situation, where we have several tens of both positive and negative plasma components, as described e.g. by the ion chemistry model of section 3.

The validity of the interpretation of incoherent scatter data in paper [6], based on expressions (3) and (4), can easily be checked if information on ion concentrations is available. A single check is made here using the data presented in paper [6]. The ion concentrations given in paper [6] in figure 9, the corresponding temperatures in figure 8, and the neutral densities corresponding to the chosen temperatures, may be used as input values in expression (1). Then we may compare the resulting spectra, as a function of altitude, with the Lorentzian shape using the spectral widths given by expression (4) for the same input values.

Spectra at selected altitudes, using data from paper [6] at 0005 UT on 14 August 1989, are compared in figure 1. The night-time is specifically chosen for this comparison since dominance of negative ions over electrons was seen at several measured altitudes (paper [6], figure 8b) . The amount of different ions which are present in significant concentrations decreases strongly with increasing altitude. However, this comparison is made with the full ion-chemistry model having 24 different positive ions and 11 negative ions (see section 3) at all altitudes. Each spectrum is normalized to unity at zero frequency. The frequency axis is logarithmic to enhance the form of the ion line feature, which would appear as a narrow spike in a linear scale.

The form of spectra from expression (1) is seen to follow closely the Lorentzian form at all altitudes.

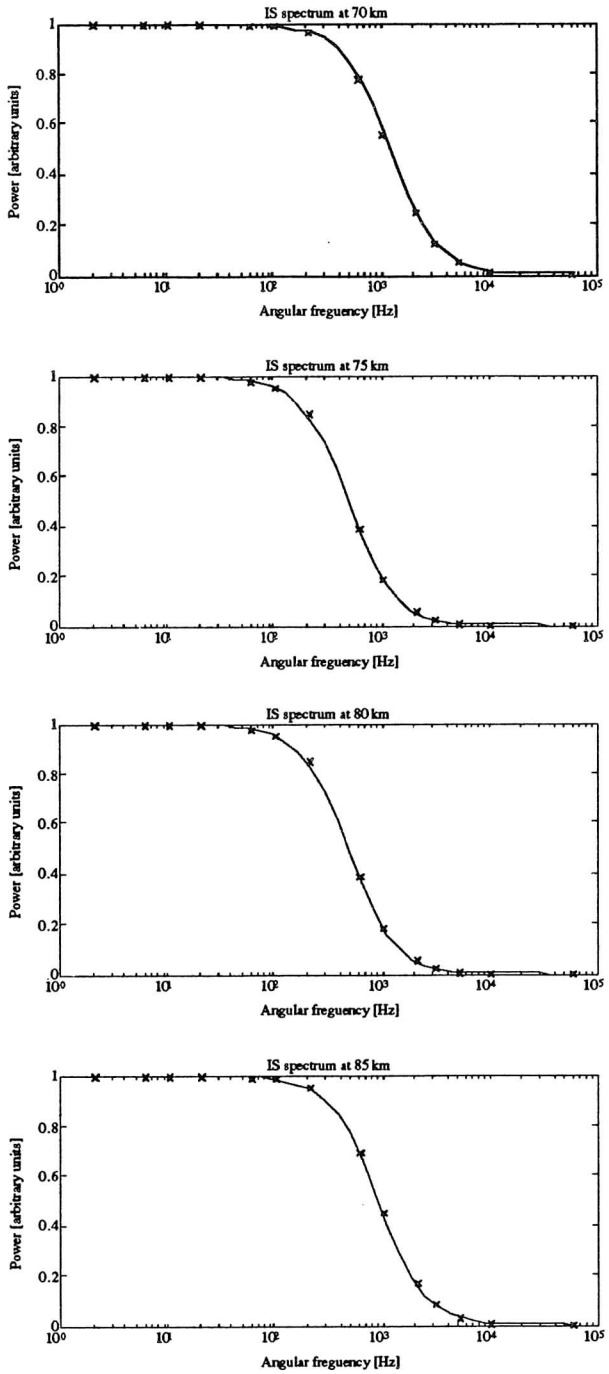


*Figure 1. Lorentzian spectra defined by spectral widths resulting from expression (4) (solid lines) and spectra from expression (1) (calculated points shown by crosses), corresponding to the input data presented in paper [6] at 0005 UT on 14 August 1989.*

A direct comparison of spectral widths between the full description by expression (1) and the one based on the mean ion mass in expression (4) is possible when a Lorentzian form is fitted to the full description spectral points in figure 1. The resulting spectral widths, as a function of altitude, are compared with the ones obtained from expression (4) in figure 2, in the left panel. The right panel

shows a similar comparison based on the ion concentration data at 0255 Ut on 14 August 1989, when negative ions are present only in negligible amounts.

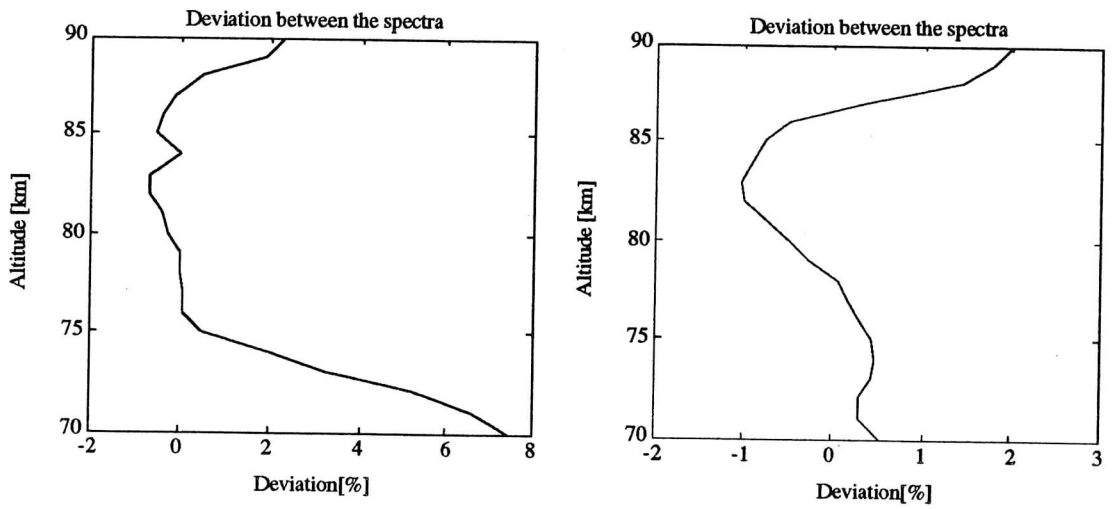


*Figure 2. Relative difference of the spectral width calculated using expression (4) from the spectral width given by a Lorentzian least squares fit to the spectral points from expression (1), presented in figure 1., for 0005 UT on 14 August 1989 (left panel) and for 0255 UT on 14 August 1989 (right panel).*

For the description of D-region by the ion chemistry model of section 3, in the example cases presented in paper [6], we see an excellent match between the spectral widths resulting from expressions (1) and (4). The relative deviation between the spectral widths is of the order of a couple of percent at all altitudes. Some significant difference seems to appear at the lowest altitude when negative ions are present during night-time.

In conclusion, the use of expression (4) with a mean ion mass description seems justified during typical D-region conditions. However, deviations between expressions (1) and (4) will occur in the presence of extraordinary heavy ion masses or multiply charged ions.

## 3. D-REGION ION CHEMISTRY MODEL

The D-region ion-chemistry model, Sodankylä Ion Chemistry (SIC) model, which is used in papers [5] and [6], is outlined in paper [5] and described in detail by Turunen et al. (1992). A shortened, self-contained description of the SIC-model is given below.

The SIC-model is effectively a 1-dimensional steady state model, which calculates ion and electron concentrations in ionospheric D- and lower E-regions. Originally the model was developed for applications during geophysically quiet conditions. Consequently, as ionisation sources acting on five primary neutral components $N_2$, $O_2$, $O$, $NO$ and $O_2(^1\Delta_g)$, the solar radiation at wavelength range 5-134 nm and galactic cosmic rays were considered. At present however, the model is extended to also include electron precipitation as ionisation source, as described by Turunen et al. (1992). A similar extension is the use of the model during solar proton events, as in the application of the SIC-model in paper [6].

The altitude range of the SIC-model is chosen to be from 70 to 100 km, which corresponds to the measurement range of the most common EISCAT incoherent scatter radar D-region experiments. The assumptions on which the model is based are summarized below:

1) The neutral atmosphere is described by the semi-empirical model MSIS-86 (Hedin, 1987).

2) The ionospheric D-region is sunlit. This restricts the range for solar zenith angle to be below about 95 degrees.

3) Ionisation during quiet time is primarily caused by photoionisation and galactic cosmic rays.

4) We neglect any transport effects. Photoequilibrium can be assumed since the chemical lifetimes of the ions are short with respect to transport processes.

5) The concentrations of neutral species are much higher than those of ions and thus assumed to be unaffected by ion chemistry.

6) An overall charge neutrality prevails.

In addition to the above mentioned neutrals, also $Ar$, $He$ and $CO_2$ are included in photoionisation calculations, because they absorb the solar radiation at the relevant wavelength range. To account for important ion-chemical reactions we need to include also $H_2O$, $N$, $H$, $O_3$, $OH$, $NO_2$ and $HO_2$ in the list of neutral components in the model. The height distributions of the main constituents of the neutral air, $N_2$, $O_2$, $O$, $Ar$, $He$, $H$ and $N$, and the height profile of the neutral temperature were adopted from the MSIS-86 model (Hedin, 1987). Since the altitude range of this model is limited from below by the mesopause, the values are extrapolated below this limiting altitude as described by Alcaydé (1981). This extrapolation needs information on stratopause temperature and height.

For those neutral constituents which are not covered by the MSIS-86 model ($NO$, $O_2(^1\Delta^g)$, $CO_2$, $H_2O$, $O_3$, $OH$, $NO_2$, $HO_2$) fixed reference profiles are used. Since the atmospheric composition in the considered altitude region is mainly controlled by turbulent mixing, also fixed mixing ratios of $3 \cdot 10^4$ and $1 \cdot 10^6$ for $CO_2$ and $H_2O$, respectively, can be used. It depends on the application of the model which of the above mentioned minor constituent profiles are fixed and which are varied. Examples of reference minor constituent concentration profiles are given in figure 3.

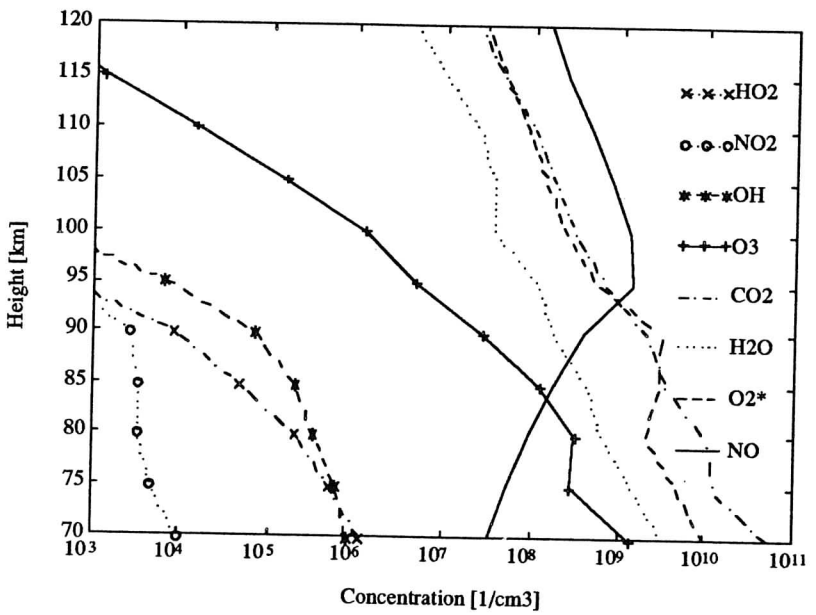


*Figure 3. Selected example profiles for neutral constituents not covered by MSIS-86 model.*

Photoionisation at altitude $h$, for solar zenith angle $\chi$, is calculated using the following expression:

$$q_j(\chi,h) = \int_\lambda I_\infty(\lambda) e^{-\sum_k \sigma_k(\lambda) \int_h^\infty N_k Ch(h,\chi)\, dh} \eta_j(\lambda)\sigma_j(\lambda) n_j(h)\, d\lambda \quad , \tag{5}$$

where

$q_j(\chi,h)$ = photoionization rate for neutral component j ,

$I_\infty(\lambda)$ = intensity of the solar radiation outside the atmosphere ,

$\sigma_k(\lambda)$ = absorption cross-section for neutral component k ,

$Ch(h,\chi)$ = grazing incidence function ,

$\eta_j(\lambda)$ = photoionization efficiency for neutral component j ,

and

$$n_j(h) = \text{concentration of neutral component j .}$$

The exponential function in expression (5) describes the absorption of solar radiation at each wavelength. The grazing incidence function accounts for the earth's curvature. The integral in the exponent is calculated numerically using expressions (Rees, 1989):

$$\int_{h_o}^{\infty} n_j(h)Ch(h,\chi)\,dh = \int_{h_o}^{\infty} n_j(h)\left[1-\left(\frac{R+h_o}{R+h}\right)^2 \sin^2\chi\right]^{-\frac{1}{2}} dh \qquad \text{, for } \chi < 90° \qquad (6a)$$

and

$$\int_{h_o}^{\infty} n_j(h)Ch(h,\chi)\,dh = 2\int_{h_{min}}^{\infty} n_j(h)\left[1-\left(\frac{R+h_{min}}{R+h}\right)^2\right]^{-\frac{1}{2}} dh - \int_{h_o}^{\infty} n_j(h)\left[1-\left(\frac{R+h_o}{R+h}\right)^2 \sin^2\chi\right]^{-\frac{1}{2}} dh \qquad \text{, for } \chi > 90°, \qquad (6b)$$

where

$$R = \text{Earth radius}$$

and

$$h_{min} = cos(\chi - 90°)(h_o + R) - R \quad \text{is the minimum height along photon path.}$$

Absorption cross-sections for $N_2$, $O_2$, $O$ and $He$ are from Torr et al. (1979), for $NO$ and $Ar$ the constants from the tables of Ohshio et al. (1966) are used, and for $CO_2$ the data are from McEwan and Phillips (1975). Photoionisation efficiencies come from the same references as the absorption cross-sections. The absorption cross-sections and photoionisation efficiencies are listed in table 1.

A reference solar spectrum was collected from the spectrum by Torr et al. (1979) and from spectrum $R74113$ by Heroux and Hinteregger (1978). The intensities for wavelengths 103.76 nm and 110.8 nm were taken from the paper of Huffman et al. (1971). For our reference spectrum $Ly\text{-}\alpha$ line was chosen from Lean and Skumanich (1983). The intensities can be varied according to the chosen level of solar activity. The reference spectrum for the value $F_{10.7} = 68$ is also given in table 1.

| Wave-length [nm] | Intens. $10^9$ cm$^{-2}$s$^{-1}$ | Abs. cross sect. (cm$^{-2}$) $N_2$ | $O_2$ | $O$ | $Ar$ | $He$ | $NO$ | $O_2$ ($^1\Delta^g$) | $CO_2$ | Ion. eff. $N_2$ | $O_2$ | $O$ | $Ar$ | $He$ | $NO$ | $O_2$ ($^1\Delta^g$) |
|---|---|---|---|---|---|---|---|---|---|---|---|---|---|---|---|---|
| 5-10 | 0.3834 | 6.00e-19 | 1.18e-18 | 1.06e-18 | 0 | 2.10e-19 | 0 | 0 | 0 | 1.00 | 1.00 | 1.00 | 6.16 | 1.00 | 0 | 0 |
| 10-15 | 0.1346 | 2.32e-18 | 3.61e-18 | 3.53e-18 | 0 | 5.30e-19 | 0 | 0 | 0 | 1.00 | 1.00 | 1.00 | 3.50 | 1.00 | 0 | 0 |
| 15-20 | 1.8418 | 5.40e-18 | 7.27e-18 | 5.96e-18 | 0 | 1.02e-18 | 0 | 0 | 0 | 1.00 | 1.00 | 1.00 | 2.54 | 1.00 | 0 | 0 |
| 20-25 | 0.9235 | 8.15e-18 | 1.05e-17 | 7.55e-18 | 0 | 1.71e-18 | 0 | 0 | 0 | 1.00 | 1.00 | 1.00 | 0.22 | 1.00 | 0 | 0 |
| 25.63 | 0.2713 | 9.65e-18 | 1.28e-17 | 8.43e-18 | 0 | 2.16e-18 | 0 | 0 | 0 | 1.00 | 1.00 | 1.00 | 0 | 1.00 | 0 | 0 |
| 28.415 | 0.1 | 1.06e-17 | 1.48e-17 | 9.26e-18 | 0 | 2.67e-18 | 0 | 0 | 0 | 1.00 | 1.00 | 1.00 | 0 | 1.00 | 0 | 0 |
| 25-30 | 0.8405 | 1.01e-17 | 1.36e-17 | 8.78e-18 | 0 | 2.38e-18 | 0 | 0 | 0 | 1.00 | 1.00 | 1.00 | 0 | 1.00 | 0 | 0 |
| 30.331 | 0.235 | 1.16e-17 | 1.60e-17 | 9.70e-18 | 0 | 3.05e-18 | 0 | 0 | 0 | 1.00 | 1.00 | 1.00 | 0 | 1.00 | 0 | 0 |
| 30.378 | 6 | 1.16e-17 | 1.60e-17 | 9.72e-18 | 0 | 3.05e-18 | 0 | 0 | 0 | 1.00 | 1.00 | 1.00 | 0 | 1.00 | 0 | 0 |
| 30-35 | 0.8661 | 1.46e-17 | 1.72e-17 | 1.00e-17 | 0 | 3.65e-18 | 0 | 0 | 0 | 1.00 | 1.00 | 1.00 | 0 | 1.00 | 0 | 0 |
| 36.807 | 0.7394 | 1.80e-17 | 1.84e-17 | 1.08e-17 | 0 | 4.35e-18 | 0 | 0 | 0 | 1.00 | 1.00 | 1.00 | 0 | 1.00 | 0 | 0 |
| 35-40 | 0.2121 | 1.75e-17 | 1.82e-17 | 1.07e-17 | 0 | 4.25e-18 | 0 | 0 | 0 | 1.00 | 1.00 | 1.00 | 0 | 1.00 | 0 | 0 |
| 40-45 | 0.3926 | 2.11e-17 | 1.94e-17 | 1.12e-17 | 0 | 5.51e-18 | 0 | 0 | 0 | 1.00 | 1.00 | 1.00 | 0 | 1.00 | 0 | 0 |
| 46.522 | 0.18 | 2.18e-17 | 2.04e-17 | 1.13e-17 | 2.99e-17 | 6.53e-18 | 0 | 0 | 0 | 1.00 | 1.00 | 1.00 | 0.55 | 1.00 | 0 | 0 |
| 45-50 | 0.3063 | 2.18e-17 | 2.16e-17 | 1.16e-17 | 2.47e-17 | 7.09e-18 | 0 | 0 | 0 | 1.00 | 1.00 | 1.00 | 0.44 | 1.00 | 0 | 0 |
| 50-55 | 0.5085 | 2.45e-17 | 2.41e-17 | 1.19e-17 | 3.68e-17 | 7.20e-19 | 0 | 0 | 0 | 1.00 | 1.00 | 1.00 | 0.55 | 1.00 | 0 | 0 |
| 55.437 | 0.7992 | 2.47e-17 | 2.56e-17 | 1.21e-17 | 3.81e-17 | 0 | 0 | 0 | 0 | 1.00 | 1.00 | 1.00 | 0.57 | 0 | 0 | 0 |
| 58.433 | 1.58 | 2.32e-17 | 2.20e-17 | 1.22e-17 | 4.32e-17 | 0 | 2.31e-17 | 0 | 0 | 1.00 | 1.00 | 1.00 | 0.71 | 0 | 0.93 | 0 |
| 55-60 | 0.4843 | 2.24e-17 | 2.50e-17 | 1.19e-17 | 3.82e-17 | 0 | 0 | 0 | 0 | 1.00 | 1.00 | 1.00 | 0.67 | 0 | 0.37 | 0 |
| 60.976 | 0.45 | 2.31e-17 | 2.61e-17 | 1.22e-17 | 4.09e-17 | 0 | 2.37e-17 | 0 | 0 | 1.00 | 1.00 | 1.00 | 0.78 | 0 | 0.96 | 0 |
| 62.973 | 1.5 | 2.32e-17 | 2.58e-17 | 1.22e-17 | 4.26e-17 | 0 | 2.37e-17 | 0 | 0 | 1.00 | 1.00 | 1.00 | 0.81 | 0 | 0.96 | 0 |
| 60-65 | 0.1746 | 2.32e-17 | 2.60e-17 | 1.22e-17 | 3.93e-17 | 0 | 2.25e-17 | 0 | 0 | 1.00 | 1.00 | 1.00 | 0.79 | 0 | 0.96 | 0 |
| 65-70 | 0.2223 | 2.98e-17 | 2.63e-17 | 1.00e-17 | 3.75e-17 | 0 | 2.07e-17 | 0 | 0 | 0.84 | 0.84 | 1.00 | 0.81 | 0 | 0.94 | 0 |
| 70.336 | 0.3915 | 2.63e-17 | 2.50e-17 | 1.13e-17 | 3.63e-17 | 0 | 2.22e-17 | 0 | 0 | 0.88 | 0.92 | 1.00 | 0.88 | 0 | 0.82 | 0 |
| 70-75 | 0.1667 | 3.09e-17 | 2.91e-17 | 8.00e-18 | 3.51e-17 | 0 | 2.06e-17 | 0 | 0 | 0.75 | 0.82 | 1.00 | 0.85 | 0 | 0.78 | 0 |
| 76.515 | 0.1997 | 3.55e-17 | 2.20e-17 | 4.18e-18 | 3.34e-17 | 0 | 1.60e-17 | 0 | 0 | 0.67 | 0.39 | 1.00 | 0.78 | 0 | 0.57 | 0 |
| 77.041 | 0.2425 | 2.69e-17 | 2.52e-17 | 4.18e-18 | 3.41e-17 | 0 | 1.60e-17 | 0 | 0 | 0.68 | 0.39 | 1.00 | 0.78 | 0 | 0.57 | 0 |
| 78.936 | 0.7931 | 1.93e-17 | 2.67e-17 | 4.28e-18 | 0 | 0 | 1.71e-17 | 0 | 0 | 0.53 | 0.41 | 1.00 | 0 | 0 | 0.56 | 0 |
| 75-80 | 0.8728 | 3.07e-17 | 2.71e-17 | 4.23e-18 | 3.10e-17 | 0 | 1.89e-17 | 0 | 0 | 0.55 | 0.35 | 1.00 | 0.70 | 0 | 0.58 | 0 |
| 80-85 | 1.9311 | 1.50e-17 | 2.09e-17 | 4.38e-18 | 0 | 0 | 1.77e-17 | 0 | 0 | 0 | 0.29 | 1.00 | 0 | 0 | 0.54 | 0 |
| 85-90 | 4.4325 | 4.66e-17 | 9.85e-18 | 4.18e-18 | 0 | 0 | 2.71e-17 | 0 | 0 | 0 | 0.48 | 1.00 | 0 | 0 | 0.47 | 0 |
| 90-95 | 4.217 | 1.70e-17 | 1.55e-17 | 2.12e-18 | 0 | 0 | 3.38e-17 | 0 | 0 | 0 | 0.60 | 1.00 | 0 | 0 | 0.45 | 0 |
| 97.702 | 5.957 | 7.00e-19 | 4.00e-18 | 0 | 0 | 0 | 1.96e-17 | 0 | 0 | 0 | 0.63 | 0 | 0 | 0 | 0.55 | 0 |
| 95-100 | 1.785 | 3.62e-17 | 1.65e-17 | 0 | 0 | 0 | 1.99e-17 | 0 | 0 | 0 | 0.74 | 0 | 0 | 0 | 0.55 | 0 |
| 102.572 | 4.375 | 0 | 1.60e-18 | 0 | 0 | 0 | 1.94e-17 | 0 | 0 | 0 | 0.63 | 0 | 0 | 0 | 0.52 | 0 |
| 100-102.7 | 1.112 | 0 | 1.10e-18 | 0 | 0 | 0 | 2.08e-17 | 0 | 0 | 0 | 0.25 | 0 | 0 | 0 | 0.55 | 0 |
| 103.191 | 3.184 | 0 | 1.12e-18 | 0 | 0 | 0 | 1.38e-17 | 5.52e-18 | 0 | 0 | 0 | 0 | 0 | 0 | 0.62 | 1.00 |
| 103.761 | 1.63 | 0 | 1.08e-18 | 0 | 0 | 0 | 1.30e-17 | 5.14e-18 | 0 | 0 | 0 | 0 | 0 | 0 | 0.65 | 1.00 |
| 102.7-105 | 0.898 | 0 | 1.10e-18 | 0 | 0 | 0 | 1.16e-17 | 5.16e-18 | 0 | 0 | 0 | 0 | 0 | 0 | 0.66 | 1.00 |
| 105-110 | 2.8 | 0 | 9.50e-19 | 0 | 0 | 0 | 8.89e-18 | 4.81e-18 | 1.63e-17 | 0 | 0 | 0 | 0 | 0 | 0.79 | 1.00 |
| 110.8 | 0.24 | 0 | 5.00e-21 | 0 | 0 | 0 | 4.43e-18 | 3.32e-18 | 2.30e-17 | 0 | 0 | 0 | 0 | 0 | 0.82 | 1.00 |
| 110-111.8 | 0.232 | 0 | 3.90e-19 | 0 | 0 | 0 | 4.43e-18 | 3.40e-18 | 3.48e-17 | 0 | 0 | 0 | 0 | 0 | 0.82 | 1.00 |
| 111.8-115 | 0.438 | 0 | 0 | 0 | 0 | 0 | 3.49e-18 | 0 | 0 | 0 | 0 | 0 | 0 | 0 | 0.83 | 0 |
| 115-120 | 4.4 | 0 | 0 | 0 | 0 | 0 | 2.71e-18 | 0 | 0 | 0 | 0 | 0 | 0 | 0 | 0.86 | 0 |
| 121.568 | 232 | 6.00e-23 | 9.00e-21 | 0 | 0 | 0 | 2.40e-18 | 0 | 0 | 0 | 0 | 0 | 0 | 0 | 0.81 | 0 |
| 120-125 | 8 | 0 | 3.06e-19 | 0 | 0 | 0 | 2.21e-18 | 0 | 0 | 0 | 0 | 0 | 0 | 0 | 0.76 | 0 |
| 125-130 | 4.1 | 0 | 0 | 0 | 0 | 0 | 2.27e-18 | 0 | 0 | 0 | 0 | 0 | 0 | 0 | 0.52 | 0 |
| 130-135 | 12.4 | 0 | 2.90e-18 | 0 | 0 | 0 | 2.52e-18 | 0 | 0 | 0 | 0 | 0 | 0 | 0 | 0.23 | 0 |

*Table 1. The solar spectrum corresponding to the value $F_{10.7} = 68$, absorption cross-sections and photoionisation efficiencies.*

Heaps (1978) has derived a convenient parametrization of the empirical rate of ion pair production by cosmic rays, $Q_{cr}$, as a function of latitude, altitude and solar activity level. We use this parametrization as described by the following expressions (units $s^{-1}cm^{-3}$) :

$$Q_{cr} = (X_1 + X_2 sin^4\phi) \cdot 3 \cdot 10^{17(1-X_3)} \cdot M^{X_3} \quad \text{for } M > 3 \cdot 10^{17} \text{ , } |\phi| < 53^\circ \text{ ,} \qquad (7a)$$

where

$$X_1 = 1.74 \cdot 10^{-18} \text{ ,}$$

$$X_2 = 1.93 \cdot 10^{-17} \quad \text{(solar maximum),}$$

$$X_2 = 2.84 \cdot 10^{-17} \quad \text{(solar minimum),}$$

$$X_3 = 0.6 + 0.8 \cdot |\cos\phi| \text{ ,}$$

$$M = \text{number density of air } [\frac{1}{\text{cm}^3}]$$

and

$$\phi = \text{latitude ;}$$

$$Q_{cr} = (X_1 + X_2 sin^4\phi) \cdot M \quad \text{for } M < 3 \cdot 10^{17} \text{ , } |\phi| < 53^\circ \text{ ;} \qquad (7b)$$

$$Q_{cr} = X_1 \cdot M \quad \text{for solar maximum , } |\phi| > 53^\circ \qquad (7c)$$

and

$$Q_{cr} = (X_1 + X_2) \cdot M \quad \text{for solar minimum , } |\phi| > 53^\circ \text{ ,} \qquad (7d)$$

where

$$X_1 = 1.44 \cdot 10^{-17}$$

and

$$X_2 = 4.92 \cdot 10^{-18} \text{ .}$$

This is initially taken to be effective for the major neutral components $N_2$ and $O_2$.

Description of ionisation by a given precipitating particle flux may be included using an empirically defined particle energy dissipation distribution function (Rees, 1963). The total ionisation rate due to precipitating particles is then divided between the main ionizable constituents according to the relative magnitudes of the effective ionisation cross sections and concentrations of the constituents. In order to get ion production rates suitable to be added to those by photoionisation, we must in addition account for the branching ratios between direct and dissociative ionisation processes. Denoting the ionisation rate of air due to electron precipitation by $q$, we have the following expressions (Jones, 1974; Rees, 1989) for the production rates $p_e(X)$ of ions $X$:

$$p_e(N_2^+) = 0.76 \cdot q(N_2) \quad ,$$
$$p_e(O_2^+) = 0.66 \cdot q(O_2) \tag{8}$$
and
$$p_e(O^+) = 0.33 \cdot q(O_2) + q(O) \quad ,$$
where
$$q(N_2) = q\frac{0.92n(N_2)}{0.92n(N_2) + n(O_2) + 0.56n(O)} \quad ,$$
$$q(O_2) = q\frac{n(O_2)}{0.92n(N_2) + n(O_2) + 0.56n(O)} \quad ,$$
$$q(O) = q\frac{0.56n(O)}{0.92n(N_2) + n(O_2) + 0.56n(O)}$$
and
$n(X) =$ is the concentration of neutral component $X$ .

The primary ions $N_2^+$, $O_2^+$, $O^+$, $NO^+$ and electron $e^-$ react with neutral components forming more complex ions. The SIC-model includes altogether 24 positive and 11 negative ions. These are introduced in figures 4 and 5, showing the positive and negative ions, and their mutual reactions, respectively.

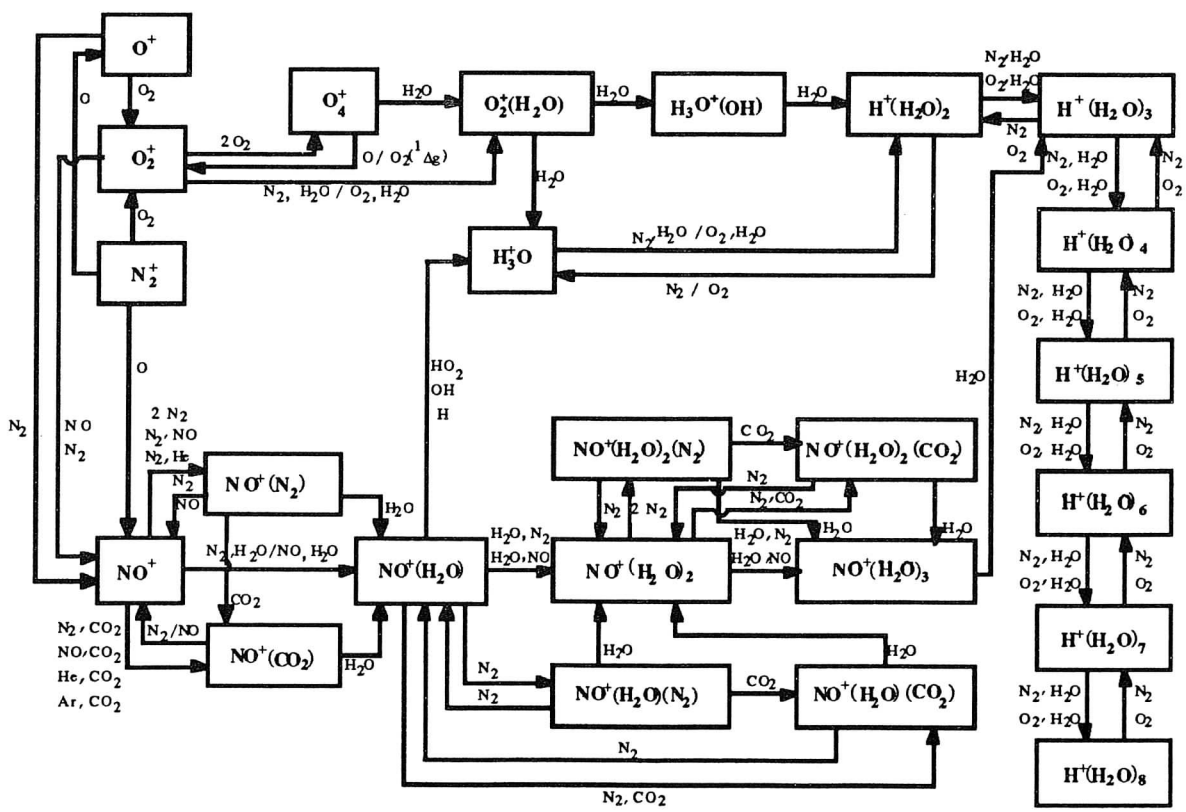


*Figure 4. SIC-model positive ion reaction scheme.*

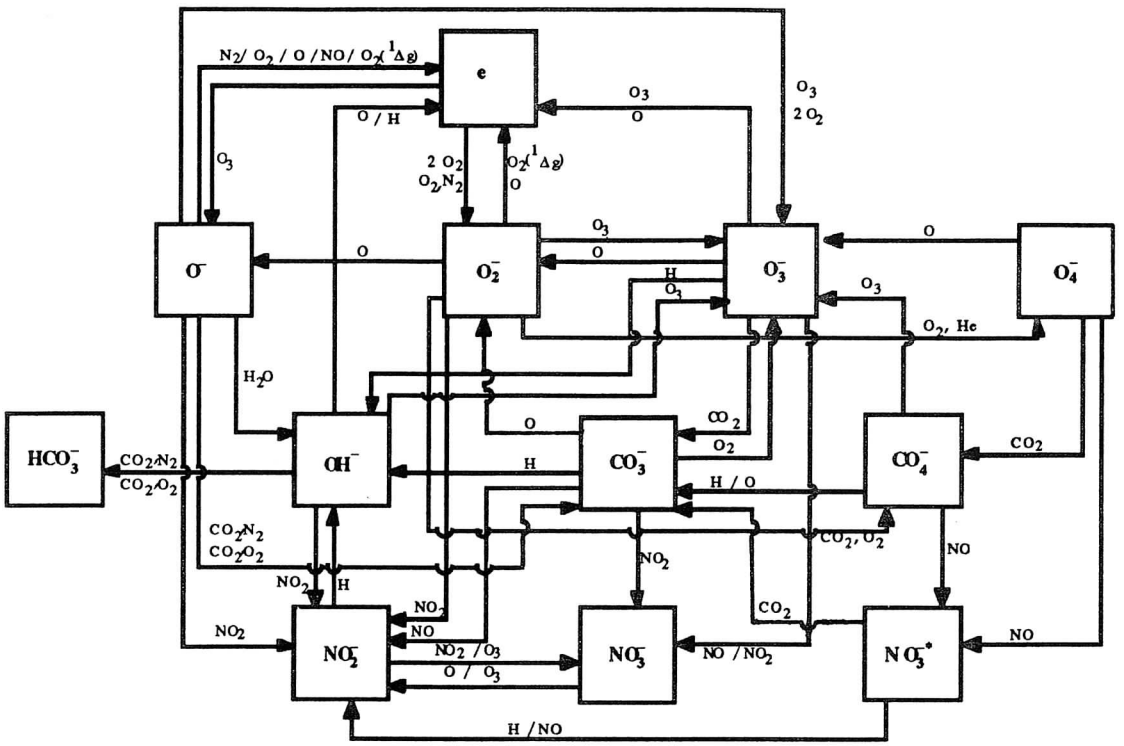


*Figure 5. SIC-model negative ion reaction scheme.*

A complete reaction list, including also recombination, photodissociation and photodetachment processes, is given in table 2. Table 2 is a collection of information from several sources. The main contributions were taken from the works by Chakrabarty et al. (1978), Wisemberg and Kockarts (1980), Torkar and Friedrich (1983) and Thomas and Bowman (1985).

| Positive ion reactions | Rate coefficients ($cm^3s^{-1}$ or $cm^6s^{-1}$) |
|---|---|
| $O^+ + O_2 \rightarrow O_2^+ + O$ | $1.5 \cdot 10^{-11}(300/T)$ /26/ |
| $O^+ + N_2 \rightarrow NO^+ + N$ | $1.2 \cdot 10^{-12}(300/T)$ /26/ |
| $O_2^+ + 2O_2 \rightarrow O_4^+ + O_2$ | $4.0 \cdot 10^{-30}(300/T)^{2.93}$ /5/ |
| $O_2^+ + NO \rightarrow NO^+ + O_2$ | $4.4 \cdot 10^{-10}$ /3/ |
| $O_2^+ + N_2 \rightarrow NO^+ + NO$ | $5 \cdot 10^{-16}$ /20/ |
| $O_2^+ + N_2 + H_2O \rightarrow O_2^+(H_2O) + N_2$ | $2.8 \cdot 10^{-28}$ /3/ |
| $O_2^+ + O_2 + H_2O \rightarrow O_2^+(H_2O) + O_2$ | $2.3 \cdot 10^{-28}$ /3/ |
| $O_4^+ + O \rightarrow O_2^+ + O_3$ | $3 \cdot 10^{-10}$ /3/ |
| $O_4^+ + O_2(^1\Delta_g) \rightarrow O_2^+ + 2O_2$ | $> 10^{-10}$ /13/ |
| $O_4^+ + H_2O \rightarrow O_2^+(H_2O) + O_2$ | $1.8 \cdot 10^{-9}$ /3/ |
| $N_2^+ + O \rightarrow O^+ + N_2$ | $9.8 \cdot 10^{-12}(300/T)^{0.23}$ /11/ |
| $N_2^+ + O_2 \rightarrow O_2^+ + N_2$ | $5 \cdot 10^{-11}(300/T)^{0.8}$ /26/ |
| $N_2^+ + O \rightarrow NO^+ + N$ | $1.4 \cdot 10^{-10}(300/T)^{0.44}$ /11/ |
| $NO^+ + N_2 + NO \rightarrow NO^+(N_2) + NO$ | $2 \cdot 10^{-31}(300/T)^{0.44}$ /21/ |
| $NO^+ + N_2 + He \rightarrow NO^+(N_2) + He$ | $2 \cdot 10^{-31}(300/T)^{0.44}$ /21/ |
| $NO^+ + 2N_2 \rightarrow NO^+(N_2) + N_2$ | $2 \cdot 10^{-31}(300/T)^{0.44}$ /21/ |
| $NO^+ + N_2 + CO_2 \rightarrow NO^+(CO_2) + N_2$ | $7 \cdot 10^{-30}(300/T)^3$ /21/ |
| $NO^+ + NO + CO_2 \rightarrow NO^+(CO_2) + NO$ | $7 \cdot 10^{-30}(300/T)^3$ /21/ |
| $NO^+ + He + CO_2 \rightarrow NO^+(CO_2) + He$ | $7 \cdot 10^{-30}(300/T)^3$ /21/ |
| $NO^+ + Ar + CO_2 \rightarrow NO^+(CO_2) + Ar$ | $3.0 \cdot 10^{-29}$ /9/ |
| $NO^+ + N_2 + H_2O \rightarrow NO^+(H_2O) + N_2$ | $1.8 \cdot 10^{-28}(308/T)^{4.7}$ /21/ |
| $NO^+ + NO + H_2O \rightarrow NO^+(H_2O) + NO$ | $1.8 \cdot 10^{-28}(308/T)^{4.7}$ /21/ |
| $NO^+(N_2) + N_2 \rightarrow NO^+ + 2N_2$ | $1.5 \cdot 10^6 T^{-5.4} \exp(-2450/T)$ /21/ |
| $NO^+(N_2) + NO \rightarrow NO^+ + N_2 + NO$ | $1.5 \cdot 10^6 T^{-5.4} \exp(-2450/T)$ /21/ |
| $NO^+(N_2) + CO_2 \rightarrow NO^+(CO_2) + N_2$ | $1 \cdot 10^{-9}$ /27/ |
| $NO^+(N_2) + H_2O \rightarrow NO^+(H_2O) + N_2$ | $1 \cdot 10^{-9}$ /21/ |
| $NO^+(CO_2) + N_2 \rightarrow NO^+ + CO_2 + N_2$ | $3.1 \cdot 10^4 T^{-4} \exp(-4590/T)$ /21/ |
| $NO^+(CO_2) + NO \rightarrow NO^+ + CO_2 + NO$ | $3.1 \cdot 10^4 T^{-4} \exp(-4590/T)$ /21/ |
| $NO^+(CO_2) + H_2O \rightarrow NO^+(H_2O) + CO_2$ | $1 \cdot 10^{-9}$ /21/ |
| $NO^+(H_2O) + H_2O + N_2 \rightarrow NO^+(H_2O)_2 + N_2$ | $1 \cdot 10^{-27}(308/T)^{4.7}$ /21/ |
| $NO^+(H_2O) + H_2O + NO \rightarrow NO^+(H_2O)_2 + NO$ | $1 \cdot 10^{-27}(308/T)^{4.7}$ /21/ |
| $NO^+(H_2O) + 2N_2 \rightarrow NO^+(H_2O)(N_2) + N_2$ | $2 \cdot 10^{-31}(300/T)^{4.4}$ /21/ |
| $NO^+(H_2O) + N_2 + CO_2 \rightarrow NO^+(H_2O)(CO_2) + N_2$ | $7 \cdot 10^{-30}(300/T)^3$ /21/ |
| $NO^+(H_2O) + HO_2 \rightarrow H^+(H_2O) + NO_3$ | $< 10^{-9}$ /12/ |
| $NO^+(H_2O) + OH \rightarrow H^+(H_2O) + NO_2$ | $1 \cdot 10^{-10}$ /3/ |
| $NO^+(H_2O) + H \rightarrow H^+(H_2O) + NO$ | $7 \cdot 10^{-12}$ /12/ |
| $NO^+(H_2O)_2 + H_2O + N_2 \rightarrow NO^+(H_2O)_3 + N_2$ | $1.9 \cdot 10^{-27}(308/T)^{4.7}$ /21/ |
| $NO^+(H_2O)_2 + H_2O + NO \rightarrow NO^+(H_2O)_3 + NO$ | $1.9 \cdot 10^{-27}(308/T)^{4.7}$ /21/ |
| $NO^+(H_2O)_2 + 2N_2 \rightarrow NO^+(H_2O)_2(N_2) + N_2$ | $2 \cdot 10^{-31}(300/T)^{4.4}$ /21/ |
| $NO^+(H_2O)_2 + N_2 + CO_2 \rightarrow NO^+(H_2O)_2(CO_2) + N_2$ | $7 \cdot 10^{-30}(300/T)$ /21/ |
| $NO^+(H_2O)_3 + H_2O \rightarrow H^+(H_2O)_3 + HNO_2$ | $7 \cdot 10^{-11}$ /21/ |
| $NO^+(H_2O)(N_2) + N_2 \rightarrow NO^+(H_2O) + 2N$ | $1.5 \cdot 10^6 T^{-5.4} \exp(-2150/T)$ /21/ |
| $NO^+(H_2O)(N_2) + H_2O \rightarrow NO^+(H_2O)_2 + N_2$ | $1 \cdot 10^{-9}$ /21/ |
| $NO^+(H_2O)(N_2) + CO_2 \rightarrow NO^+(H_2O)(CO_2) + N_2$ | $1 \cdot 10^{-9}$ /21/ |
| $NO^+(H_2O)(CO_2) + N_2 \rightarrow NO^+(H_2O) + N_2 + CO_2$ | $3.1 \cdot 10^4 T^{-4} \exp(-4025/T)$ /21/ |
| $NO^+(H_2O)(CO_2) + H_2O \rightarrow NO^+(H_2O)_2 + CO_2$ | $1 \cdot 10^{-9}$ /21/ |
| $NO^+(H_2O)_2(N_2) + N_2 \rightarrow NO^+(H_2O)_2 + 2N_2$ | $1.5 \cdot 10^6 T^{-5.4} \exp(-1800/T)$ /21/ |
| $NO^+(H_2O)_2(N_2) + H_2O \rightarrow NO^+(H_2O)_3 + N_2$ | $1.0 \cdot 10^{-9}$ /21/ |
| $NO^+(H_2O)_2(N_2) + CO_2 \rightarrow NO^+(H_2O)_2(CO_2) + N_2$ | $1 \cdot 10^{-9}$ /21/ |
| $NO^+(H_2O)_2(CO_2) + N_2 \rightarrow NO^+(H_2O)_2 + N_2 + CO_2$ | $3.1 \cdot 10^4 T^{-4} \exp(-3335/T)$ /21/ |
| $NO^+(H_2O)_2(CO_2) + H_2O \rightarrow NO^+(H_2O)_3 + CO_2$ | $1 \cdot 10^{-9}$ /21/ |
| $O_2^+(H_2O) + H_2O \rightarrow H_3O^+(OH) + O_2$ | $1.4 \cdot 10^{-9}$ /3/ |
| $O_2^+(H_2O) + H_2O \rightarrow H^+(H_2O) + OH + O_2$ | $2.4 \cdot 10^{-10}$ /3/ |
| $H_3O^+(OH) + H_2O \rightarrow H^+(H_2O)_2 + OH$ | $2.0 \cdot 10^{-9}$ /3/ |
| $H^+(H_2O) + N_2 + H_2O \rightarrow H^+(H_2O)_2 + N_2$ | $3.4 \cdot 10^{-27}(300/T)^4$ /21/ |
| $H^+(H_2O) + O_2 + H_2O \rightarrow H^+(H_2O)_2 + O_2$ | $3.4 \cdot 10^{-27}(300/T)^4$ /21/ |
| $H^+(H_2O)_2 + N_2 \rightarrow H^+(H_2O) + H_2O + N_2$ | $9.6 \cdot 10^{11} T^{-5} \exp(-17100/T)$ /21/ |
| $H^+(H_2O)_2 + O_2 \rightarrow H^+(H_2O) + H_2O + O_2$ | $9.6 \cdot 10^{11} T^{-5} \exp(-17100/T)$ /21/ |
| $H^+(H_2O)_2 + N_2 + H_2O \rightarrow H^+(H_2O)_3 + N_2$ | $2.3 \cdot 10^{-27}(300/T)^4$ /21/ |
| $H^+(H_2O)_2 + O_2 + H_2O \rightarrow H^+(H_2O)_3 + O_2$ | $2.3 \cdot 10^{-27}(300/T)^4$ /21/ |
| $H^+(H_2O)_3 + N_2 \rightarrow H^+(H_2O)_2 + H_2O + N_2$ | $2.0 \cdot 10^{11} T^{-5} \exp(-11000/T)$ /21/ |
| $H^+(H_2O)_3 + O_2 \rightarrow H^+(H_2O)_2 + H_2O + O_2$ | $2.0 \cdot 10^{11} T^{-5} \exp(-11000/T)$ /21/ |
| $H^+(H_2O)_3 + N_2 + H_2O \rightarrow H^+(H_2O)_4 + N_2$ | $2.4 \cdot 10^{-27}(300/T)^4$ /21/ |
| $H^+(H_2O)_3 + O_2 + H_2O \rightarrow H^+(H_2O)_4 + O_2$ | $2.4 \cdot 10^{-27}(300/T)^4$ /21/ |
| $H^+(H_2O)_4 + N_2 \rightarrow H^+(H_2O)_3 + H_2O + N_2$ | $1.4 \cdot 10^{11} T^{-5} \exp(-8360/T)$ /21/ |
| $H^+(H_2O)_4 + O_2 \rightarrow H^+(H_2O)_3 + H_2O + O_2$ | $1.4 \cdot 10^{11} T^{-5} \exp(-8360/T)$ /21/ |
| $H^+(H_2O)_4 + N_2 + H_2O \rightarrow H^+(H_2O)_5 + N_2$ | $9 \cdot 10^{-28}(300/T)^4$ /21/ |
| $H^+(H_2O)_4 + O_2 + H_2O \rightarrow H^+(H_2O)_5 + O_2$ | $9 \cdot 10^{-28}(300/T)^4$ /21/ |
| $H^+(H_2O)_5 + N_2 \rightarrow H^+(H_2O)_4 + H_2O + N_2$ | $6.9 \cdot 10^{11} T^{-5} \exp(-7670/T)$ /21/ |
| $H^+(H_2O)_5 + O_2 \rightarrow H^+(H_2O)_4 + H_2O + O_2$ | $6.9 \cdot 10^{11} T^{-5} \exp(-7670/T)$ /21/ |
| $H^+(H_2O)_5 + N_2 + H_2O \rightarrow H^+(H_2O)_6 + N_2$ | $9 \cdot 10^{-28}(300/T)^4$ /21/ |
| $H^+(H_2O)_5 + O_2 + H_2O \rightarrow H^+(H_2O)_6 + O_2$ | $9 \cdot 10^{-28}(300/T)^4$ /21/ |
| $H^+(H_2O)_6 + N_2 \rightarrow H^+(H_2O)_5 + H_2O + N_2$ | $2.1 \cdot 10^{11} T^{-5} \exp(-6540/T)$ /21/ |
| $H^+(H_2O)_6 + O_2 \rightarrow H^+(H_2O)_5 + H_2O + O_2$ | $2.1 \cdot 10^{11} T^{-5} \exp(-6540/T)$ /21/ |
| $H^+(H_2O)_6 + N_2 + H_2O \rightarrow H^+(H_2O)_7 + N_2$ | $9 \cdot 10^{-28}(300/T)^4$ /21/ |
| $H^+(H_2O)_6 + O_2 + H_2O \rightarrow H^+(H_2O)_7 + O_2$ | $9 \cdot 10^{-28}(300/T)^4$ /21/ |
| $H^+(H_2O)_7 + N_2 \rightarrow H^+(H_2O)_6 + H_2O + N_2$ | $7.9 \cdot 10^{10} T^{-5} \exp(-5830/T)$ /21/ |
| $H^+(H_2O)_7 + O_2 \rightarrow H^+(H_2O)_6 + H_2O + O_2$ | $7.9 \cdot 10^{10} T^{-5} \exp(-5830/T)$ /21/ |
| $H^+(H_2O)_7 + N_2 + H_2O \rightarrow H^+(H_2O)_8 + N_2$ | $9 \cdot 10^{-28}(300/T)^4$ /21/ |
| $H^+(H_2O)_7 + O_2 + H_2O \rightarrow H^+(H_2O)_8 + O_2$ | $9 \cdot 10^{-28}(300/T)^4$ /21/ |
| $H^+(H_2O)_8 + N_2 \rightarrow H^+(H_2O)_7 + H_2O + N_2$ | $2.3 \cdot 10^{10} T^{-5} \exp(-5000/T)$ /21/ |
| $H^+(H_2O)_8 + O_2 \rightarrow H^+(H_2O)_7 + H_2O + O_2$ | $2.3 \cdot 10^{10} T^{-5} \exp(-5000/T)$ /21/ |

| Recombination of positive ions with electron | Rate coefficients ($cm^3s^{-1}$) |
|---|---|
| $O^+ + e \rightarrow O$ | $4.0 \cdot 10^{-12}(300/Te)^{0.7}$ /29/ |
| $O_2^+ + e \rightarrow O + O$ | $1.9 \cdot 10^{-7}(300/Te)^{0.5}$ /17/ |
| $N_2^+ + e \rightarrow N_2$ | $3.5 \cdot 10^{-7}(300/Te)^{0.5}$ /17/ |
| $NO^+ + e \rightarrow N + O$ | $2.3 \cdot 10^{-7}(300/Te)^{0.5}$ /17/ |
| $NO^+(N_2) + e \rightarrow NO + N_2$ | $2.0 \cdot 10^{-6}(300/Te)^{0.5}$ /4/ |
| $NO^+(CO_2) + e \rightarrow NO + CO_2$ | $1.5 \cdot 10^{-6}$ /26/ |
| $NO^+(H_2O) + e \rightarrow NO + H_2O$ | $2.0 \cdot 10^{-6}$ /12/ |
| $NO^+(H_2O)_2 + e \rightarrow NO + 2H_2O$ | $3.0 \cdot 10^{-6}$ /26/ |
| $NO^+(H_2O)_3 + e \rightarrow NO + 3H_2O$ | $4.5 \cdot 10^{-6}$ /26/ |
| $NO^+(H_2O)(N_2) + e \rightarrow NO + H_2O + N_2$ | $3.0 \cdot 10^{-6}$ /14/ |
| $NO^+(H_2O)(CO_2) + e \rightarrow NO + H_2O + CO_2$ | $3.0 \cdot 10^{-6}$ /14/ |
| $NO^+(H_2O)_2(N_2) + e \rightarrow NO + 2H_2O + N_2$ | $3.0 \cdot 10^{-6}$ /14/ |
| $NO^+(H_2O)_2(CO_2) + e \rightarrow NO + 2H_2O + CO_2$ | $3.0 \cdot 10^{-6}$ /14/ |
| $O_2^+(H_2O) + e \rightarrow O_2 + H_2O$ | $3.0 \cdot 10^{-6}$ /14/ |
| $H_3O^+(OH) + e \rightarrow$ neutrals | $3.0 \cdot 10^{-6}$ /14/ |
| $H^+(H_2O) + e \rightarrow H + H_2O$ | $5 \cdot 10^{-6}(300/Te)^{1.5}$ /6/ |
| $H^+(H_2O)_2 + e \rightarrow H + 2H_2O$ | $5 \cdot 10^{-6}(300/Te)^{1.5}$ /6/ |
| $H^+(H_2O)_3 + e \rightarrow H + 3H_2O$ | $4.0 \cdot 10^{-6}$ /4/ |
| $H^+(H_2O)_4 + e \rightarrow H + 4H_2O$ | $< 10^{-5}(300/Te)$ /4/ |
| $H^+(H_2O)_5 + e \rightarrow H + 5H_2O$ | $< 10^{-5}(300/Te)$ /4/ |
| $H^+(H_2O)_6 + e \rightarrow H + 6H_2O$ | $< 10^{-5}(300/Te)$ /4/ |
| $H^+(H_2O)_7 + e \rightarrow H + 7H_2O$ | $1.0 \cdot 10^{-5}$ /4/ |
| $H^+(H_2O)_8 + e \rightarrow H + 8H_2O$ | $1.0 \cdot 10^{-5}$ /4/ |

| Photodissociation of positive ions | Rate coefficients ($s^{-1}$) |
|---|---|
| $O_2^+(H_2O) + h\nu \rightarrow O_2^+ + H_2O$ | 0.42 /23/ |

| Negative ion reactions | Rate coefficients ($cm^3s^{-1}$ or $cm^6s^{-1}$) |
|---|---|
| $O^- + N_2 \rightarrow O + N_2 + e$ | $< 10^{-12}$ /3/ |
| $O^- + O_2 \rightarrow O + O_2 + e$ | $< 10^{-12}$ /3/ |
| $O^- + O \rightarrow O_2 + e$ | $1.9 \cdot 10^{-10}$ /3/ |
| $O^- + NO \rightarrow NO_2 + e$ | $2.1 \cdot 10^{-10}$ /3/ |
| $O^- + O_2(^1\Delta_g) \rightarrow O_3 + e$ | $3 \cdot 10^{-10}$ /3/ |

*Table 2. Ion-chemical reactions and reaction rates in the SIC-model.*

| | |
|---|---|
| $O^- + O_3 \rightarrow O_3^- + O$ | $8.0 \cdot 10^{-10}$ /3/ |
| $O^- + 2O_2 \rightarrow O_3^- + O_2$ | $1.4 \cdot 10^{-30}$ /18/ |
| $O^- + H_2O \rightarrow OH^- + OH$ | $6.0 \cdot 10^{-13}$ /3/ |
| $O^- + CO_2 + N_2 \rightarrow CO_3^- + N_2$ | $2.0 \cdot 10^{-28}$ /3/ |
| $O^- + CO_2 + O_2 \rightarrow CO_3^- + O_2$ | $2.0 \cdot 10^{-28}$ /3/ |
| $O^- + NO_2 \rightarrow NO_2^- + O$ | $1.0 \cdot 10^{-9}$ /3/ |
| $O_2^- + O \rightarrow O_3 + e$ | $1.5 \cdot 10^{-10}$ /3/ |
| $O_2^- + O_2(^1\Delta_g) \rightarrow 2O_2 + e$ | $2 \cdot 10^{-10}$ /3/ |
| $O_2^- + O \rightarrow O^- + O_2$ | $1.5 \cdot 10^{-10}$ /3/ |
| $O_2^- + O_3 \rightarrow O_3^- + O_2$ | $6 \cdot 10^{-10}$ /3/ |
| $O_2^- + O_2 + He \rightarrow O_4^- + He$ | $3.4 \cdot 10^{-31}$ /3/ |
| $O_2^- + CO_2 + O_2 \rightarrow CO_4^- + O_2$ | $4.7 \cdot 10^{-29}$ /3/ |
| $O_2^- + NO_2 \rightarrow NO_2^- + O_2$ | $7 \cdot 10^{-10}$ /3/ |
| $O_3^- + O \rightarrow 2O_2 + e$ | $1 \cdot 10^{-10}$ /15/ |
| $O_3^- + O_3 \rightarrow 3O_2 + e$ | $1 \cdot 10^{-10}$ /1/ |
| $O_3^- + O \rightarrow O_2^- + O_2$ | $2.5 \cdot 10^{-10}$ /3/ |
| $O_3^- + H \rightarrow OH^- + O_2$ | $8.4 \cdot 10^{-10}$ /3/ |
| $O_3^- + CO_2 \rightarrow CO_3^- + O_2$ | $5.5 \cdot 10^{-10}$ /3/ |
| $O_3^- + NO \rightarrow NO_3^- + O$ | $2.6 \cdot 10^{-12}$ /3/ |
| $O_3^- + NO_2 \rightarrow NO_3^- + O_2$ | $2.8 \cdot 10^{-10}$ /3/ |
| $O_4^- + O \rightarrow O_3^- + O_2$ | $4 \cdot 10^{-10}$ /3/ |
| $O_4^- + CO_2 \rightarrow CO_4^- + O_2$ | $4.3 \cdot 10^{-10}$ /3/ |
| $O_4^- + NO \rightarrow NO_3^{-*} + O_2$ | $2.5 \cdot 10^{-10}$ /3/ |
| $OH^- + O \rightarrow HO_2 + e$ | $2 \cdot 10^{-10}$ /3/ |
| $OH^- + H \rightarrow H_2O + e$ | $1.4 \cdot 10^{-9}$ /3/ |
| $OH^- + O_3 \rightarrow O_3^- + OH$ | $9 \cdot 10^{-10}$ /3/ |
| $OH^- + NO_2 \rightarrow NO_2^- + OH$ | $1.1 \cdot 10^{-9}$ /3/ |
| $OH^- + CO_2 + N_2 \rightarrow HCO_3^- + N_2$ | $7.6 \cdot 10^{-28}$ /3/ |
| $OH^- + CO_2 + O_2 \rightarrow HCO_3^- + O_2$ | $7.6 \cdot 10^{-28}$ /3/ |
| $CO_3^- + O \rightarrow O_2^- + CO_2$ | $1.1 \cdot 10^{-10}$ /3/ |
| $CO_3^- + O_2 \rightarrow O_3^- + CO_2$ | $6.0 \cdot 10^{-15}$ /3/ |
| $CO_3^- + H \rightarrow OH^- + CO_2$ | $1.7 \cdot 10^{-10}$ /3/ |
| $CO_3^- + NO \rightarrow NO_2^- + CO_2$ | $1.1 \cdot 10^{-11}$ /3/ |
| $CO_3^- + NO_2 \rightarrow NO_3^- + CO_2$ | $2 \cdot 10^{-10}$ /3/ |
| $CO_4^- + O_3 \rightarrow O_3^- + O_2 + CO_2$ | $1.3 \cdot 10^{-10}$ /3/ |
| $CO_4^- + H \rightarrow CO_3^- + OH$ | $2.2 \cdot 10^{-10}$ /3/ |
| $CO_4^- + O \rightarrow CO_3^- + O_2$ | $1.4 \cdot 10^{-10}$ /3/ |
| $CO_4^- + NO \rightarrow NO_3^{-*} + CO_2$ | $4.8 \cdot 10^{-11}$ /3/ |
| $NO_2^- + H \rightarrow OH^- + NO$ | $3 \cdot 10^{-10}$ /3/ |
| $NO_2^- + NO_2 \rightarrow NO_3^- + NO$ | $2 \cdot 10^{-13}$ /3/ |
| $NO_2^- + O_3 \rightarrow NO_3^- + O_2$ | $1.2 \cdot 10^{-10}$ /3/ |
| $NO_3^- + O \rightarrow NO_2^- + O_2$ | $< 1 \cdot 10^{-11}$ /3/ |
| $NO_3^- + O_3 \rightarrow NO_2^- + 2O_2$ | $1 \cdot 10^{-13}$ /3/ |
| $NO_3^{-*} + CO_2 \rightarrow CO_3^- + NO_2$ | $1.0 \cdot 10^{-11}$ /3/ |
| $NO_3^{-*} + H \rightarrow NO_2^- + OH$ | $7.2 \cdot 10^{-10}$ /3/ |
| $NO_3^{-*} + NO \rightarrow NO_2^- + NO_2$ | $1.5 \cdot 10^{-11}$ /2/ |

| Electron photodetachment of negative ions | Rate coefficients ($s^{-1}$) |
|---|---|
| $O^- + h\nu \rightarrow O + e$ | 1.4 /19/ |
| $O_2^- + h\nu \rightarrow O_2 + e$ | $3.8 \cdot 10^{-1}$ /19/ |
| $O_3^- + h\nu \rightarrow O_3 + e$ | $4.7 \cdot 10^{-2}$ /7/ |
| $OH^- + h\nu \rightarrow OH + e$ | 1.1 /7/ |
| $CO_3^- + h\nu \rightarrow CO_3 + e$ | $2.2 \cdot 10^{-2}$ /16/ |
| $NO_2^- + h\nu \rightarrow NO_2 + e$ | $8.0 \cdot 10^{-4}$ /9/ |
| $NO_3^- + h\nu \rightarrow NO_3 + e$ | $5.2 \cdot 10^{-2}$ /24/ |

| Photodissociation of negative ions | Rate coefficients ($s^{-1}$) |
|---|---|
| $O_3^- + h\nu \rightarrow O^- + O_2$ | 0.47 /8/ |
| $O_4^- + h\nu \rightarrow O_2^- + O_2$ | 0.24 /8/ |
| $CO_3^- + h\nu \rightarrow O^- + CO_2$ | 0.15 /16/ |
| $CO_4^- + h\nu \rightarrow O_2^- + CO_2$ | $6.2 \cdot 10^{-3}$ /7/ |

| Electron attachment to neutrals | Rate coefficients ($cm^3 s^{-1}$) |
|---|---|
| $O_3 + e \rightarrow O^- + O_2$ | $9.1 \cdot 10^{-12}(300/Te)^{-1.46}$ /25/ |
| $2O_2 + e \rightarrow O_2^- + O_2$ | $4 \cdot 10^{-30} \exp(-193/Te)$ /28/ |
| $O_2 + N_2 + e \rightarrow O_2^- + N_2$ | $1 \cdot 10^{-31}(300/Te)\exp(-600/Te)$ /19/ |

| Ion-ion recombination | Rate coefficients ($cm^3 s^{-1}$) |
|---|---|
| $X^+ + Y^- \rightarrow$ neutrals | $6 \cdot 10^{-8}$ /22/ |
| $NO_2^- + X^+ \rightarrow NO_2 + X$ | $1.7 \cdot 10^{-7}$ /10/ |
| $NO_3^- + X^+ \rightarrow NO_3 + X$ | $3.4 \cdot 10^{-8}$ /10/ |

References:


1. Adams and Megill. 1967
2. Adams et al., 1970
3. Albritton, 1978
4. Biondi, 1973
5. Böhringer and Arnold, 1982
6. Chakrabarty et al., 1978
7. Cosby et al., 1976
8. DNA, 1972
9. Dunkin et al., 1971
10. Eisner and Hirsh, 1971
11. McFarland et al., 1974
12. Fehsenfeld et al., 1975
13. Fehsenfeld et al., 1971
14. Huang et al., 1978
15. Lelevier and Branscomb, 1968
16. Moseley et al., 1976
17. Mul and McGowan, 1979
18. Payzant and Kebarle, 1972
19. Phelps, 1969
20. Rees, 1989
21. Reid, 1977
22. Smith et al., 1976
23. Smith et al., 1978
24. Smith et al., 1979
25. Stelman et al., 1972
26. Swider and Narcisi, 1975
27. Thomas, 1976
28. Truby, 1972
29. Whitten and Poppoff, 1971


*Table 2 continued. Ion-chemical reactions and reaction rates in the SIC-model. The references are given in paper [5].*

Our purpose is to calculate the equilibrium concentrations of the ions introduced in figures 4 and 5, under the effect of all the reactions listed in table 2 and the direct production processes described above. Additional assumptions used in the mathematical formulation of the model are the overall charge neutrality condition and an extremely low ionisation degree. The neutral concentrations can thus be considered uneffected by the ion chemistry.

A change in the concentration $n_i$ of the ion $i$ can be described by the continuity equation. Let us denote the particle production rate by $P_i$ and the loss rate by $L_i$. For a steady state condition, and neglecting the transport effects, the continuity equation simplifies to the form

$$P_i - n_i \cdot L_i = 0 \quad , \tag{9}$$

where

$$P_i = \sum_{production\ processes\ k} p_{ik} \tag{10a}$$

and

$$L_i = \sum_{loss\ processes\ k} l_{ik} \quad . \tag{10b}$$

The charge neutrality condition reads:

$$N_e = \sum_{positive} n_i \; - \sum_{negative} n_i \quad . \tag{11}$$

In order to describe the chemical production terms $p_{ik}$ and loss terms $l_{ik}$ in expressions (10a) and (10b), let us consider a single reaction where ion $C^+$ is formed when the ion $A^+$ reacts with the neutral component B:

$$A^+ + B \rightarrow C^+ + D \quad . \tag{12}$$

If the reaction rate constant of process (12) is denoted by $k$, the ion $C^+$ is produced with rate $p_{C^+12} = k[A^+][B]$ and the ion $A^+$ is lost at the same rate $l_{A^+12} = k[A^+][B]$. When assuming that the neutral concentrations are much larger than the ion concentrations, and are not effected by the changes in ion concentrations, it is practical to define a new reaction rate constant, where the usual rate constant is multiplied by the relevant neutral concentration. Thus the production of ion $C^+$ and loss of ion $A^+$ can be described by the constants $\Pi_{C^+}$ and $\Lambda_{A^+}$ in expressions

$$p_{C^+12} = \Pi_{C^+12}[A^+] \tag{13a}$$

and

$$l_{A^+12} = \Lambda_{A^+12}[A^+] \quad . \tag{13b}$$

If all the processes were linear in the unknown variables (the ion concentrations $n_i$), one could write equations (9) for each ion as a group of linear coupled equations expressed in matrix form as

$$B\vec{N} + \vec{Q} = \vec{0} \quad , \tag{14}$$

where B is a 35x35 matrix having as its elements the terms $\Pi$ and $\Lambda$, which describe the production and loss rates of each ion. $\vec{N}$ is a vector containing the 35 unknown ion concentrations. $\vec{Q}$ is a vector which contains the constant production rates from expressions (5), (7) and (8).

Writing equation (14) in element form as

$$\begin{pmatrix} -\Lambda_1 & & & \\ & -\Lambda_2 & (\Pi) & \\ & & \ddots & \\ & (\Pi) & & -\Lambda_n \end{pmatrix} \begin{pmatrix} n_1 \\ n_2 \\ \vdots \\ n_n \end{pmatrix} + \begin{pmatrix} p_{11} + p_{12} \\ p_{21} + p_{22} \\ \vdots \\ p_{n1} + p_{n2} \end{pmatrix} = \vec{0} \tag{15}$$

we can assign the contributions from different types of the involved processes to the elements in equation (15), as described in table 3.

| Process type | Reaction | production rate of ion k ($i \rightarrow k$) | loss rate of ion i | location B | | Q |
|---|---|---|---|---|---|---|
| | | | | bki | bii | qk |
| Photoionization | $A + h\nu \rightarrow A^+ + e^-$ | $p_{k1}$ | | | | $p_{k1}$ |
| Galactic cosmic rays | $A + E \rightarrow A^+ + e^-$ | $p_{k2}$ | | | | $p_{k2}$ |
| Positive ion reactions | $A^+ + M \rightarrow B^+ + N$ | $\Pi_{ki}$ | $\Lambda_i$ | $\Pi_{ki}$ | $-\Lambda_i$ | — |
| Negative ion reactions | $A^- + M \rightarrow B^- + N$ | $\Pi_{ki}$ | $\Lambda_i$ | $\Pi_{ki}$ | $-\Lambda_i$ | — |
| | $A^- + M \rightarrow AM + e^-$ | — | $\Lambda_i$ | — | $-\Lambda_i$ | — |
| | $A^- + M \rightarrow A + M + e^-$ | — | $\Lambda_i$ | — | $-\Lambda_i$ | — |
| Positive ion dissociation | $AM^+ + h\nu \rightarrow A^+ + M$ | $\Pi_{ki}$ | $\Lambda_i$ | $\Pi_{ki}$ | $-\Lambda_i$ | — |
| Negative ion dissociation | $CM^- + h\nu \rightarrow C^- + M$ | $\Pi_{ki}$ | $\Lambda_i$ | $\Pi_{ki}$ | $-\Lambda_i$ | — |
| Negative ion photodetachment | $B^- + h\nu \rightarrow B + e^-$ | — | $\Lambda_i$ | — | $-\Lambda_i$ | — |

*Table 3. Location of production and loss terms in equation (15). Only two direct production processes are shown. Ionisation by electron or proton flux contributes similarily as galactic cosmic rays.*

The diagonal elements $\Lambda_i$ in the matrix in equation (15) are the sums of all the loss rates of ion $i$. The non-diagonal elements are seemingly single production rates in separate processes, but sometimes one ion may be formed from the same source ion through a few different reactions with different neutrals, in which case also the production rate could be a composite one.

If we express the electron concentration using the charge neutrality condition (11), equation (14) is missing the processes which make our set of simultaneous coupled equations nonlinear. These are the positive ion recombination with electron, recombination reactions between positive and negative ions and the negative ion formation by electron attachment to neutrals. The effect of these processes in equation (15) is described in table 4.

| Process type | Reaction | effect on elements | dependence introduced B | dependence introduced Q |
|---|---|---|---|---|
| Positive ion recombination | $A^+ + e^- \rightarrow A$ | $\Lambda_i \rightarrow \Lambda_i + \alpha_i N_e$ | $B \rightarrow B(N)$ | |
| Ion-ion recombination | $X^+ + X^- \rightarrow$ neutrals | $\Lambda_i \rightarrow \Lambda_i + \xi_i \sum_{pos} n_{pos}$<br>$\Lambda_i \rightarrow \Lambda_i + \eta_i \sum_{neg} n_{neg}$ | $B \rightarrow B(N)$ | |
| Electron attachment | $A + e^- \rightarrow A^-$ | $q_i \rightarrow q_i + \gamma_i N_e$ | | $Q \rightarrow Q(N)$ |

*Table 4. Processes introducing nonlinearity in equation (15).*

The equilibrium condition, including all the processes described in tables 3 and 4, can now be expressed in a simple form

$$\vec{F}(\vec{N}) = B(\vec{N})\,\vec{N} + \vec{Q}(\vec{N}) = \vec{0} \quad , \tag{16}$$

where the elements of the matrix B and vector Q are given by tables 2, 3 and 4 together with information on neutral concentrations.

We solve equation (16) using the Newton-Raphson method (see e.g. Press et al., 1986). Let us denote by vector $\vec{N}$ the solution of equation (16) and by $\vec{N}_o$ some initial guess of the solution. We may write

$$\vec{N} = \vec{N}_o + \vec{\delta} \quad , \tag{17}$$

where $\vec{\delta}$ is the correction vector needed to bring $\vec{N}_o$ to be the real solution $\vec{N}$.

In the neighbourhood of $\vec{N}_o$ each component $f_i$ of function $\vec{F}$ may be written as a Taylor series expansion

$$f_i(\vec{N}_o + \vec{\delta}) = f_i(\vec{N}_o) + \sum_j \left(\frac{\partial f_i}{\partial N_j}\right)_{\vec{N}=\vec{N}_o} \cdot \delta_j + \ldots = 0 \quad . \tag{18}$$

If we suppose that the guess $\vec{N}_o$ is sufficiently near the solution $\vec{N}$, we may neglect the second and higher order terms in expression (18). Thus we get a linear equation for each component of the correction vector $\vec{\delta}$ in the form

$$\sum_j \left(\frac{\partial f_i}{\partial N_j}\right)_{\vec{N}=\vec{N}_o} \cdot \delta_j = -f_i(\vec{N}_o) \quad . \tag{19}$$

From equation (16), the components $f_i$ of the function $\vec{F}$ may be written in the form $f_i(\vec{N}) = \sum B_{ij}(\vec{N}) n_j + q_i(\vec{N})$. The partial derivatives of the components $f$ with respect to the ion concentrations $n$ can then be expressed as

$$\left(\frac{\partial f_i}{\partial n_k}\right)_{\vec{N}=\vec{N}_o} = \left(\sum_j \frac{\partial B_{ij}(\vec{N})}{\partial n_k} n_j + B_{ik}(\vec{N}) + \frac{\partial q_i(\vec{N})}{\partial n_k}\right)_{\vec{N}=\vec{N}_o} \quad . \tag{20}$$

The partial derivatives (20) can be written in a simple explicit form by defining vectors $\vec{G}^+$, $\vec{G}^-$ and $\vec{G}^e$ which identify the positive and negative ions and their charges. The components of these vectors are given by expressions

$$g_i^+ = \begin{cases} 1, & \text{for } i \leq 24 \\ 0, & \text{for } i \geq 25 \end{cases} \quad , \tag{21a}$$

$$g_i^- = \begin{cases} 0, & \text{for } i \leq 24 \\ 1, & \text{for } i \geq 25 \end{cases} \tag{21b}$$

and

$$\vec{G}^e = \vec{G}^+ - \vec{G}^- \quad . \tag{21c}$$

The total electron and ion concentrations are then $N_e = \vec{G}^e \cdot \vec{N}$, $N^+ = \vec{G}^+ \cdot \vec{N}$ and $N^- = \vec{G}^- \cdot \vec{N}$.

Using the coefficients defined in tables 2, 3 and 4, the partial derivatives are given by the expression

$$\left(\frac{\partial f_i}{\partial n_k}\right)_{\vec{N}=\vec{N}_o} = (-\alpha_i g_k^e - \xi_i g_k^+ - \eta_i g_k^-)(\vec{N}_o)_i + B_{ik}(\vec{N}_o) + \gamma_i g_k^e \quad . \tag{22}$$

The linear group of equations (19) is solved using the singular value decomposition method which makes it possible to check any improper behaviour of the set of equations.

Once the equation for the correction vector $\vec{\delta}$ is solved, we have from expression (17) a new value $\vec{N}' = \vec{N}_o + \vec{\delta}$ for the guess of the unknown ion concentrations $\vec{N}$. If our initial guess $\vec{N}_o$ was good enough, the new guess $\vec{N}'$ is nearer to the solution $\vec{N}$. By solving again for a correction vector $\vec{\delta}'$ we form an iterative procedure, which gives an approximation of the solution $\vec{N}$. The numerical accuracy of the solution could be controlled, for example, by the components of the vector $\vec{\delta}$, satisfying the condition $\sqrt{\sum_i \delta_i^2} < \varepsilon$, where $\varepsilon$ is a number defining the desired numerical accuracy.

In practice, for the SIC-model procedure we use the behaviour of the components of the vector function $\vec{F}$ as the criterion to stop the iteration. If the iteration converges the elements $f_i$ give direct information about how good a solution we have found for each equation. The initial guess for the solution must be sensible to make the iteration to converge. Since the amount of important ion species rapidly decreases with increasing altitude, a trial solution is first formed for the lowest altitude, where all included ions are present. Having an initial solution for the lowest height we solve the equations (16) and continue with the next height in a 1 km grid, always using as the initial guess the final solution for the previous height.

# 4. ANALYSIS OF INCOHERENT SCATTER MEASUREMENTS

The analysis of incoherent scatter measurements in E- and F-regions has been well developed over the years. Even theoretical parameter error estimation of the inverse problem has been presented by Vallinkoski (1988). In D-region work one encounters severe difficulties in instrumentation and experiment design due to properties of the target. First, the ionisation is extremely low, resulting in very weak signals, which are difficult to separate from mere noise. Second, receiver recovery effects, and other similar effects often disturb measurements at the lowest altitudes. These effects include operation of receiver protection switches, transmitter pulse leakage to receiver front end, behaviour of noise temperature and gain after the transmitter pulse, and the strong atmospheric clutter. Third, the incoherent scatter spectrum at D-region altitudes is so narrow that the sampling time of the autocorrelation function, needed to resolve the spectrum, becomes comparable to interpulse separation times in the transmitted pulse train. This will cause clutter from higher altitudes, where the signals are orders of magnitude higher. All this results in a complicated experiment design structure, which should reduce data distortions and where a balance between different unwanted effects should be found (Turunen, 1986).

The radar equation (2) allows straightforward estimation of electron density from the scattered power. If ionisation in the target region is low, only the zero time lag of the autocorrelation function may be above the detection threshold, and the whole spectrum is not resolved. Time integration of the sampled data may help to resolve the spectrum. But at the same time we will loose the time resolution, which is needed to solve the physical problems which the experiment was aimed at.

In the D-region the incoherent scatter spectrum is expected to have a Lorentzian form, whose Fourier-transform is an exponential. From figure 1 the characteristic times of the exponentials are seen to be at least a few milliseconds at the lowest D-region altitudes. Because recovery times are of the order of only tens of microseconds, a simple way to get rid of the recovery effects is to replace the zero time lag of the autocorrelation function estimate with a lag of about 100 $\mu$s.

Paper [1] discusses determination of the effective recombination coefficient of the D-region during a solar proton event. EISCAT incoherent scatter data on electron density and GOES-5 satellite data on proton flux were used. The EISCAT experiment, with code name ESLA-T4, was a Barker-coded multipulse experiment (Turunen and Silén, 1984). The zero lag of a multipulse experiment is ambiguous in range. In ESLA-T4 separate single pulses at different frequency channels are used to estimate the zero lag. The electron density was estimated initially with time resolution of one minute and height gate separation of 600 m at altitudes above 63 km, using expression (2).

Below altitude 80 km the recovery effects were reduced by replacing the zero lag of the auto-correlation function by the lag 104 $\mu$s. The effect of this correction is most clearly seen in figure 5 of paper [1]. Incremental absorption of cosmic radio noise at 30 MHz was calculated from the estimated electron density. Without the correction the incremental absorption would approach infinity at the lowest altitudes, since electron-neutral collision frequency is increasing exponentially with decreasing altitude. The absorption profile at 1030 UT shows that high ionisation in the beginning of the proton

event occurs below the lowest altitude of the EISCAT experiment.

The incoherent scatter signal from D-region was very weak. The experiment ESLA-T4 was not specifically designed for D-region applications, but as a high resolution sporadic E-layer experiment. The data shown in figures 3 and 5 of paper [1] are the result of time averaging over 10 minutes.

The statistical accuracy of the single pulse power profiles is increased when information present in the multipulse zero lag is used. The range ambiquity can be removed using an inversion approach presented by Lehtinen and Huuskonen (1986). This method was applied for altitudes above 80 km.

The estimated values of electron density were compared with cosmic radio noise absorption measurements at 30 MHz. This comparison is presented in figure 6 of paper [1]. The recordings by a standard wide beam riometer antenna are reduced to a zenithal value by a factor of 0.83 (Hargreaves et al., 1979). A general agreement of the calculated and observed absorption is seen for the electron-neutral collision frequency profile by Kane (1961). However, at the beginning of the proton event the calculated absorption is higher than the measured one by almost a factor of two. This is surprising, since normally one would expect the high ionization below EISCAT range coverage to result in lower calculated absorption. The origin of the deviation remains unclear.

There are two known sources of error in the electron density values, arising from the possible presence of negative ions and from the effect of a finite electron Debye length. These are not included in expression (2). As seen from expression (3) the electron density will be overestimated due to the first effect, but underestimated due to the second, and both effects become greater at lower heights. No further corrections were tried for the electron density data in paper [1], since knowledge about negative ions in the form of a reliable model, or spectral width information, would have been necessary. Moreover, only the two lowest altitudes in the estimation of the effective recombination rate were subject to this uncertainty in the absolute values.

The interpretation of EISCAT electron density data in the form of effective recombination rates was performed in the following way.

The proton flux measurements in the solar wind, by the satellite GOES-5, were used to calculate ion production rates in the lower ionosphere. The calculation was done using the computer algorithm "PROTON" by G. Reid (private communication). The algorithm includes experimental data on proton energy dissipation and a fixed neutral atmosphere density profile at the relevant altitudes. Values of $\alpha_{eff} = \frac{q}{N_e^2}$ were calculated for every 5 km between altitudes 65 and 90 km and for each half hour between 1030 and 1330 UT on 16 February, 1984, except for 1130 UT when the EISCAT antenna was pointed away from zenith. The results of this analysis are described in section 5.

A special D-region experiment for EISCAT UHF and VHF radars, with code name GEN-11, was developed to overcome the technical difficulties mentioned above (Turunen, 1986). This experiment is widely used (e.g. papers [3], [4], [5], [6]; Hall et al., 1987, 1988; Collis et al., 1988; Hoppe et al., 1988; Risbeth et al., 1988; Hall and Brekke, 1988) and it is today one of the EISCAT routine experiments. Paper [2] contains a description of the range ambiguities produced by the transmitted modulation and describes the treatment of the received signal. Paper [2] also describes in detail how these ambiguities are removed and suggests a method to remove clutter from the lowest altitudes.

The experiment GEN-11 is a pulse to pulse correlation experiment for the EISCAT UHF and VHF radars. It uses 13-bit Barker-coded double pulses with a total length of 91 $\mu$s each, and a time delay between the two pulses varying cyclically between 7 and 35 $\mu$s in steps of 7 $\mu$s. One transmission cycle consists of 70 double pulses at a time interval of 2.222 ms, from which 22 lags are calculated. The modulation is designed to remove background noise, mains harmonic contamination and F-region clutter automatically from the autocorrelation function estimates. Data is received for 42 range gates, with separation 1.05 km. The measured range extends from 70 km to 113.05 km.

The use of pulse pairs inevitably produces range ambiguities. Also the zero lag estimate which in fact is a nominal lag of 112 $\mu$s is ambiguous in range. These ambiguities can be described conveniently by the theory of ambiguity functions for incoherent scatter experiments as described by Lehtinen (1986). In incoherent scatter experiments time lagged products of the complex signal are calculated to yield the autocorrelation function estimate of the signal. The estimate of a lagged product is given as a weighted average of the plasma autocorrelation function both in the lag variable $\nu$ and spatial variable $\vec{x}$. The weighting is specified by a two-dimensional weighting function, power at receiver input and receiver input impedance. If the plasma autocorrelation function is constant in $\nu$, within the region where the ambiguity function is non-zero, the ambiguity function is reduced to a one-dimensional range ambiguity function. It tells the weights of the different altitude ranges in the estimate and is determined solely by the receiver impulse response and the transmitted modulation. In Barker-coded experiments the receiver impulse response is the convolution of the impulse response of the post-detection filter with that of the Barker-decoder.

The range ambiguities of the experiment GEN-11 are presented in figures 4 and 5 of paper [2]. The effect of the ambiguities is different for different lags. The total area of the ambiguities, compared with the response from the measured altitude, ranges from 11 % to 56 %. A simple solution to the ambiguity problem would be to use only those lags with the minimum ambiguities in estimation of the spectra. However, once the ambiguity functions are exactly known, the results of an unambiguous measurement can be simulated using a correction procedure described by Huuskonen et al. (1988). The procedure results in a set of experiment-specific correction matrices, by which the altitude profiles of the measured lags have to be multiplied. An example of these matrices is given as figure 6 of paper [2].

In order to study the effect of the range ambiguity removal, data measured by the EISCAT VHF radar on 27 April 1987 between 2210 and 2230 UT was analysed. An exponential fit to the measured autocorrelation function was done, introducing additional parameters to describe the Doppler shift due to plasma drift and lag dependent clutter at the lowest altitudes. Uncorrected and corrected autocorrelation functions are presented in figure 8 of paper [2], and results of fits for uncorrected and corrected data are shown in figure 9 of paper [2]. The correlation time in figure 9 of paper [2] is the inverse of the Lorentzian spectral width. Above 90 km the correlation times based on the uncorrected data are consistently about 20 % higher than the corrected values, but between 80 and 90 km the difference is small. Below 80 km the difference is again greater and increases with decreasing altitude, finally reaching values up to a factor of two. The effects of the correction on estimated values of physical parameters in D-region are discussed in section 5.

Paper [3] describes results from the experiment GEN-11 with EISCAT UHF radar on 1 July 1985, between 1954 UT and 2134 UT. The range ambiguity correction described above was applied to the original radar data. At the very lowest altitudes the corrected lag of 112 $\mu$s is a good approximation of

the received power, but at other altitudes an additional correction must be made. When the spectrum can be assumed to be Lorentzian, one can use the extrapolation obtained by fitting an exponential curve to the measured autocorrelation function points. This assumption however fails in the upper D-region. A solution, adopted in paper [3], is to use model autocorrelation functions in the vicinity of the zero lag to correct the values to a true power estimate. Figure 6 shows an altitude dependent correction factor for the EISCAT UHF radar, obtained from model autocorrelation functions presented by Schlegel (1979). At higher altitudes this method will also fail, due to bandwidth limitation of the experiment and increasing effect of inaccuracy in the model autocorrelation function. Examination of the data in papers [2] and [3] shows that the limiting altitudes, for UHF and VHF radars respectively, are slightly above 90 km and around 100 km.

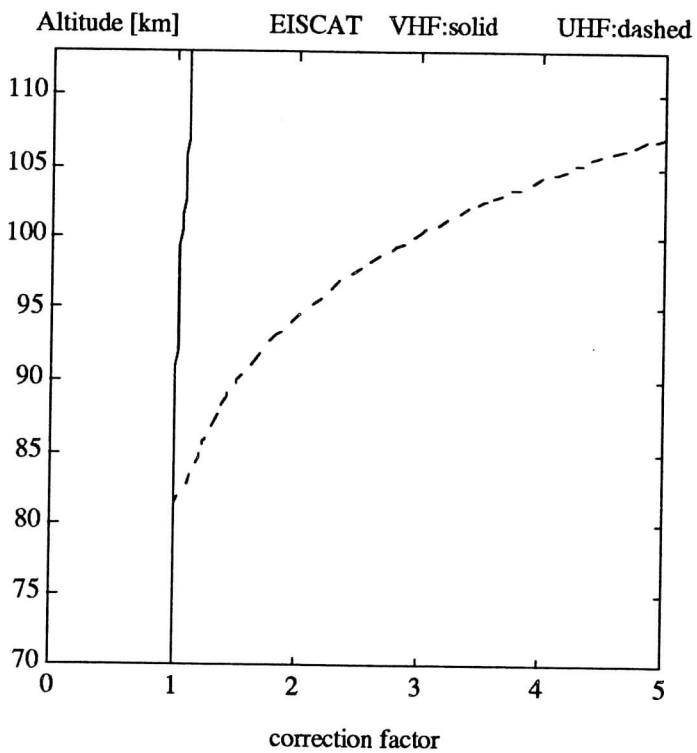


*Figure 6. Correction factors to estimate true power from lag 112 μs in GEN-11 experiment for the EISCAT VHF (solid line) and UHF (dashed line) radars.*

Electron density estimates presented in figure 2 of paper [3] were subject to one more correction. This is the Debye length correction already mentioned when discussing the possible errors in electron density values of paper [1]. From expression (3) it is seen that the raw electron density from expression (2) is in error for low values of electron density. If the D-region electron density is below $10^{10}\mathrm{m}^{-3}$, the corrected values can be up to a few tens of per cent greater than the raw values. An iterative procedure to solve for the Debye-corrected electron density was described by Mathews et al. (1982). The same treatment was used in paper [3].

The bulk motion of the plasma produces a Doppler shift to the scattered spectrum. This shift appears as a phase factor in the measured autocorrelation function. The phase may be determined

by fitting it as a separate parameter when fitting an exponential form to the measured autocorrelation function, or equivalently, when fitting a Lorentzian form to the spectrum. In paper [3] the so-called 'matched filter' method was used to determine the phase and thus plasma velocity. The measured autocorrelation function was then multiplied by the opposite phase to give a Doppler corrected autocorrelation function. An exponential fit to the corrected data was done to extract correlation time $t_c$. The correlation time depends on ion-neutral collision frequency $\nu_{in}$, ion mass $m_i$, temperature $T$ and negative ion to electron concentration ratio $\lambda$, as described by the expression

$$t_c = \frac{2.37 \cdot 10^{19} \nu_{in} m_i}{T(1+\lambda)} \quad . \tag{23}$$

Expression (23) corresponds to a simplification of expression (4). The effects of a finite Debye length are neglected here.

Figure 4 in paper [3] shows altitude profiles of vertical wind velocity with time resolution of 4 minutes during a half hour period. Clear indications of wave-like motions are seen. The velocity at a certain altitude may change by several meters per second in a few minutes. A direct consequence is that the coherence time, or spectral width, cannot be reliably estimated from raw radar data which is time integrated too long. An example of this Doppler broadening of the spectra is given in figure 6 of paper [3]. Time integration of the raw data over 30 minutes, and Doppler correction thereafter, yields from 5 to 25 % broader spectral widths, compared with the result of averaging the individually Doppler corrected 4 minutes spectra over 30 minutes. Thus all the results derived from correlation time in paper [3] were based on the individually Doppler corrected spectra.

Expression (23) was used to estimate the altitude profile of ion-neutral collision frequency from the determined correlation times. Mean ion mass of 30.5, absence of negative ions during sunlit conditions and a model temperature were assumed. The resulting ion-neutral collision frequencies and their interpretation are discussed in section 5.

The use of expressions (4) and (23) seems justified by the comparisons presented in figures 1 and 2. However, a real justification would be given by a comparison with experimental data. This was carefully tried in paper [4]. The solar proton event of August 1989 produced excess ionisation in the D-region during several days. EISCAT UHF radar was measuring with experiment GEN-11 during three nights between 12 and 15 August. The antenna was pointed cyclically in three positions. The cycle of pointing directions was vertical, to the south, vertical and to the west, with a five minutes measuring period in each direction. Antenna elevation in the two oblique positions was 72.5°, in order to get three-dimensional information of the wind field (not reported in this thesis). The radar data was analysed according to guidelines given in paper [2] to give spectral widths with time resolution of 5 minutes.

Theoretical spectral widths were calculated from expression (4) with the assumption of no negative ions present. The Debye length was approximated from the raw electron density given by expression (2). The mean ion mass was described by a selected measured altitude profile of ion mass (Johannessen and Thrane, 1974), which was adjusted to correspond to the condition of high ionisation by modifying the cluster ion concentrations, according to their recombination coefficients given by Swider and Narcisi (1975, table 1, reactions 31–34). The adopted ion mass is shown in figure 3 of

paper [4].

Empirical temperature profiles measured by a *Na* lidar experiment, run at Andøya Rocket Range 129 km west of the EISCAT site, were averaged separately over each night of measurements and also over a period of five nights. Single measured temperature profiles show significant wavelike structures. The use of average profiles was preferred, since the actual profile over the lidar site does not necessarily represent the thermal situation above EISCAT at the same time. The empirical temperature profile of Fleming et al. (1988), in the following called CIRA 88 profile, was also used. The temperatures are shown in figure 2 of paper [4]. As the lidar measurements extended only down to around 85 km, the temperatures were combined with the CIRA 88 values at 80 km and below, linearly interpolating the temperature between 80 km and the lowest (in altitude) lidar temperature available. The ion-neutral collision frequency was calculated according to Hill and Bowhill (1977), as a function of mean ion mass and neutral mass as well as neutral density. For the neutral density the 100 km altitude density value of CIRA 88 was taken as an initial value. The altitude profile was integrated from the respective combined lidar/CIRA 88 temperature profile.

Figures 6a and 7 in paper [4] show comparisons of measured and calculated spectral widths. The differences between the measured and calculated values can be interpreted as the ratio of negative ion concentration to electron concentration, as presented in figure 6b of paper [4]. However, this should physically be justified only at the lowest altitudes, where we expect the negative ions to appear. At higher altitudes, where the differences between the calculated and measured spectral widths are most prominent, no significant amounts of negative ions are observed in experiments. This discrepancy is also seen as the negative values of the negative ion to electron concentration ratio in figure 6b of paper [4]. These features, and the result of studying the D-region spectral widths published by other authors, are further discussed in section 5. Generally a discrepancy between the measured and calculated spectral widths is seen in paper [4].

The benefits of interpretation of incoherent scatter measurements in D-region by means of a chemical model were already pointed out by Mathews (1981). A step in this direction is taken in paper [5], where electron density values measured by EISCAT were used as constraints for chemical modelling, in order to deduce the neutral nitric oxide concentration in D- and lower E-regions.

EISCAT measurements on 22–23 August 1985 with the UHF radar, and on 14 August 1988 with the VHF radar, were carefully checked to select electron density profiles which correspond to geomagnetically undisturbed conditions. The UHF radar experiment used a Barker-coded power profile with a height resolution of 1.02 km. Three mean electron density profiles, with time averaging over 15 or 25 minutes, were estimated using expression (2). These corresponded to solar zenith angles 57.8°, 70.8° and 83.7°. The VHF experiment was GEN-11, but the corrections presented in paper [2] were not taken into account. This produces errors in the electron density values of the order less than 20 %. A mean profile averaged over 20 minutes and corresponding to solar zenith angle of 81.7° was selected for modelling. Because of the known inaccuracy, the VHF data were used just for reference and main emphasis in paper [5] was put on the UHF data. Altitude range for modelling was chosen to be from 80 to 120 km. The effects of finite Debye length and negative ions can thus be neglected, and the use of expression (2) is justified.

Two different and independent ion-chemistry models were used. One was the simplified six-ion scheme of Mitra and Rowe (1972) and the other was the more complete 35-ion SIC-model. The

Mitra-Rowe scheme includes explicitly ions $NO^+$, $O_2^+$, $O_4^+$ and $O_2^-$. All the cluster ions are lumped under an effective positive ion $Y^+$ and all negative ions except $O_2^-$ under an effective negative ion $X^-$.

First the solar reference spectra of the models were adjusted to fit the EISCAT electron density data at E-region altitudes for the zenith angle 57.8°. For the Mitra-Rowe model this resulted in a multiplying factor of 2.5 for the solar EUV flux, except for the Lyman-$\alpha$ flux, for which a value of $3.0 \cdot 10^{11}\mathrm{cm}^{-2}\mathrm{s}^{-1}$ was adopted. In the SIC-model the EUV flux was multiplied by factor 1.3 and the the Lyman-$\alpha$ flux was set to $2.3 \cdot 10^{11}\mathrm{cm}^{-2}\mathrm{s}^{-1}$. The same adjustment gave satisfactory agreement between the models and the observations for the other two zenith angles at altitudes above 100 km.

As an initial altitude profile of $NO$ the concentrations for quiet geophysical conditions given by Grossmann et al. (1985) were used. The concentration of $NO$ was then modified until reasonable agreement between model and observed electron density was found at all altitudes, but with emphasis on altitudes below 100 km. For the SIC-model the derived $NO$ profile was then tested at the other two zenith angles. The Mitra-Rowe model allowed faster computations and an optimum $NO$ profile was found in a cyclical fitting procedure at all zenith angles. The resulting $NO$ profiles are presented in figure 14 of paper [5] and compared with the profiles of Grossmann et al. (1985) and Meira (1971) in figure 15 of paper [5]. A considerable increase of $NO$ concentration from the initial values was needed in order to fit the models with the radar data. Both models gave the same result. The estimated $NO$ concentrations are discussed in section 5.

In paper [5] the spectral width of the incoherent scatter signal was not utilized. Expression (4) for spectral width contains several physical parameters of the D-region: mean ion mass, neutral temperature, ion-neutral collision frequency and negative ion to electron concentration ratio. A traditional solution to the problem of the indistinguishable effect of these variables on the spectrum is to use empirical models or independent physical measurements for some of the quantities, as e.g. in papers [3] and [4]. Alternatively, it is possible to add in the data interpretation a priori information of atmospheric behaviour. That is, neutral scale height may be extracted from the altitude variation of spectral width data (Tepley and Mathews, 1978).

A complementary interpretation is offered in paper [6]. Electron concentration, negative ion to electron concentration ratio, mean ion mass and neutral temperature were estimated simultaneously from expressions (3) and (4), via the use of the detailed ion chemistry scheme, presented in section 2. Ion velocity was not treated in the context of paper [6], since its effect is only to cause Doppler shift to the scattered signal. This effect is removed in the first step of data analysis, where a Lorentzian form is fitted to the signal. EISCAT data recorded during the solar proton event of August 1989 were used. Assumptions were made on neutral atmosphere composition and primary ion production, which was calculated from GOES-7 satellite measurements of proton flux in the solar wind. The basic assumption in paper [6] is that the description of incoherent scatter given in section 2 is valid. In contrast to the treatment in paper [4], the use of expressions (3) and (4) was mathematically strictly coupled in paper [6].

The measured proton fluxes are described in figure 2 of paper [6]. Assuming these to represent the flux which penetrates the atmosphere, and using the same neutral atmosphere model as is used in the SIC-model, one can calculate the ion production rate due to the proton flux. The algorithm for this calculation is originally due to Reid and was used in paper [1] with a different neutral atmosphere and

a different altitude step. At this stage temperature is also taken from the model, but later temperature is varied, and consequently also the neutral density and the ion production rate are changed. The ionisation rate of air is divided between the main neutral components similarly as in the case of electron precipitation described in section 3 by expressions (8), but assuming the cross-sections to be proportional to the atomic masses. Production rates were calculated as

$$p_p(N_2^+) = q \cdot 0.76 \cdot \frac{0.88n(N_2)}{0.88n(N_2) + n(O_2)} \quad ,$$

$$p_p(O_2^+) = q \cdot 0.67 \cdot \frac{n(O_2)}{0.88n(N_2) + n(O_2)} \tag{8}$$

and

$$p_p(O^+) = q \cdot 0.33 \cdot \frac{0.56n(O_2)}{0.88n(N_2) + n(O_2)} \quad .$$

The total ionisation rate is shown in figure 3 of paper [6]. The individual production rates were added to the photoionisation rates, although photoionisation appears to be insignificant during a proton event.

Radar data analysis is divided in two phases. First a raw data analysis is performed as described in paper [2]. In this step the scattered signal power, spectral width and neutral wind are estimated. Neutral wind is not discussed further in paper [6]. A raw electron density estimate is formed from the scattered power using expression (2).

In the next step, the raw electron density, spectral width and the ion production rates are used as input in a procedure where expressions (3) and (4) are solved simultaneously with the solution of the ion chemical equilibrium in the SIC-model. An analytical solution to expressions (3) and (4) exists for electron concentration and negative ion to electron concentration ratio as functions of mean ion mass and temperature, if the ratio of the product of the first two multiplicative terms in expression (4) to the spectral width is less than one. This solution is explicitly written down in appendix 1 of paper [6]. Mean ion mass is available through the solution of the SIC-model. Adjusting inputs of the SIC-model, one can fit the electron concentration and negative ion to electron concentration ratio resulting from expressions (3) and (4) to the ones given by the SIC-model. Strictly, one could adjust two parameters. This is however not a suitable approach to a physical problem, where one should care about the existence of a solution for a set of nonlinear equations, which already contain simplifying assumptions. Since most of the ion chemical reactions are strongly temperature dependent, temperature is selected as the parameter to be adjusted. Adjustment is done by fitting the electron density of the SIC-model to the one from expressions (3) and (4). The consistency of our description of D-region ion chemistry and incoherent scatter can then be checked by comparing the corresponding negative ion to electron concentration ratios. This results in an iterative procedure, where for each height we start with a temperature value and corresponding neutral atmosphere. Ion production rate is then calculated and the chemical equilibrium is solved to give ion concentrations and thus electron concentration, negative ion concentration and mean ion mass. The solution of expressions (3) and (4) is then compared with the electron concentration and the temperature is changed to make the process converge. Neutral density is changed according to the temperature change, by integration from a

reference point at altitude 90 km, and keeping the relative amounts of each neutral component in constant proportions.

The above procedure was applied in paper [6] at two selected times during the night 13–14 August 1989. These times were 0005 UT and 0255 UT, corresponding to solar zenith angles 95° and 86°, respectively. At 0005 UT one would expect significant amounts of negative ions to be present, while at 0255 UT they should practically be absent in the altitude range from 70 to 90 km. The input data, raw electron density, spectral width and ion production rate are shown in figure 7 of paper [6]. The deduced height profiles of electron density, negative ion to electron concentration ratio, temperature and mean ion mass are presented in figure 8 of paper [6]. One should note that the use of the ion chemistry model also results in concentration estimates for all the different ions. The results of paper [6] are further discussed in section 5.

## 5. RESULTS

Information on the effective recombination rate in D-region is highly varying in literature. This is seen in figure 9 of paper [1], where average values of the deduced recombination rate coefficients are plotted together with earlier determinations. Most of the average values fall in the range of the previous estimates, though towards the higher extremes below altitude 85 km. Since ion production by photoionisation was neglected in paper [1], the deduced values are actually too low by a few percent. This is however less than the 10 % random error due to the uncertainty in electron density values.

An interesting comparison of the deduced values can be made with those of Reagan and Watt (1976), because their estimates were also based on incoherent scatter measurements. They used the Chatanika radar in Alaska, during the solar proton event in August 1972. Variations of the effective recombination rate coefficient as a function of time at fixed altitudes are shown in figure 10 of paper [1]. A gradual decrease during the day is seen at altitudes between 70 and 85 km. This presumably indicates a progressive change in D-region chemistry. A similar feature was observed by Reagan and Watt at altitudes between 59 and 89 km, except for an intermediate range 67–72 km.

Altitude profiles of the effective recombination rate coefficient are plotted together with the ranges of values determined by Reagan and Watt in figure 11 of paper [1]. Similar values are obtained at around 80 km. Figure 11 of paper [1] also shows the recombination rates of ions $O_2^+$, $NO^+$, $(H_3O)^+$, $H^+(H_2O)_2$, $H^+(H_2O)_3$ and $H^+(H_2O)_6$ to facilitate interpretation of the profiles. At the altitude of 90 km the deduced values are closer to the theoretical value for $O_2^+$ than for $NO^+$ recombination, in contrast to the picture of the molecular ion region seen from the values of Reagan and Watt. If the steady increase of the recombination rate coefficient below 90 km down to 75 km is attributed to an increase in the ratio of hydrated ions to molecular ions, one can estimate the altitude variation of this ratio. Ratios of hydrated to simple ions based on the average values of figure 9 in paper [1] are given in table [4] of paper [1]. The altitude where the concentrations of hydrated and simple ions are equal is about 78 km. Below the altitude of 75 km the effective recombination rate is fairly constant until a sign of strong increase is seen near altitude 65 km. The constant value corresponds to the recombination coefficient of the hydrated ion $H^+(H_2O)_6$. The values by Reagan and Watt show a lower degree of hydration.

The rapid increase of the effective recombination rate coefficient below altitude of 70 km may be caused by an increasing concentration of negative ions, or by an increasing proportion of larger cluster ions, or both. The data by Reagan and Watt show a similar feature. They discussed the second explanation, but the first one cannot be ruled out. Unfortunately the EISCAT experiment discussed in paper [1] was not designed to give spectral information appropriate for investigations of negative ions.

Estimation of negative ion to electron concentration ratio was done in paper [2] in order to see the effect of the range ambiguity correction of the data. As was mentioned in section 4, the correlation time at the height of 70 km is in error by 50 % if the correction is not done. Expression (23) was used,

with a proper constant for the VHF radar, assuming an ion mass of 30.5 and relating the collision frequency to the neutral density given by the MSIS-86 model (Hedin, 1987), with altitude extension below mesopause (Alcaydé, 1981). The case study of data on 27 April 1987 at 2210–2230 UT resulted in altitude profiles of the negative ion to electron concentration ratio, which are shown in figure 9 of paper [2]. At the lowest altitudes, where the concentration of negative ions is highest, the uncorrected data gives roughly 30 % too high ratios compared with the ones resulting from corrected data. The error is decreasing rapidly with increasing altitude and is not significant at the altitude where electron and negative ion concentrations are equal. The electron density is usually underestimated without the correction and the ion velocity is affected hardly at all. At higher altitudes, where negative ions are absent, the correlation times could be erroneous by 20 % without the correction. This would effect the possible estimation of neutral temperature, density, ion mass and ion-neutral collision frequency, or parameters related to these.

Ion-neutral collision frequencies were estimated in paper [3]. Altitude profiles of collision frequency are plotted in figure 8 of paper [3] for two neutral atmosphere models at 1958–2034 UT on 1 July 1985. For comparison, the profiles from the expression $\nu_{in} = 8.92 \cdot 10^9 \rho$, where $\rho$ is the atmospheric neutral density, are also shown. The deduced collision frequencies agree well with the model frequencies, specially if one selects for higher altitudes the model MSIS-83 (Hedin, 1983), extrapolated below mesopause as presented by Alcaydé (1981), and for lower altitudes the model CIRA (1972). At altitudes around 86 km the measurements deviate from the model values by 50 %. A possible explanation for this deviation is an increase of ion mass. A possible ion could be of the type $H^+(H_2O)_n$, where $n = 2$. A mixture of any ions with mean atomic mass of about 40 would be equivalent. However, because of the low temperatures around this altitude, the proton hydrates are the most probable candidates. The good agreement between the estimated collision frequency and the CIRA model below 86 km suggests that the assumption of ion mass is probably correct. For proton hydrates this mass would result from a mean hydration index of 1.5. Alternatively, the molecular ion regime could cover all altitudes down to 75 km, as in the case expected for hard electron precipitation. Then the layer near 86 km could be composed of metallic ions of meteoric origin. Another possible interpretation is that this feature is related to the occurence of a polar mesosphere summer echo on top of an incoherently scattered signal. This would then result in narrowing of the measured spectrum, as shown for the UHF radar by Röttger et al. (1990). However, the occurence of the PMSE should be characterized by increase in the scattered power. This was not observed, except for the special feature seen at 2058–2134 UT (figure 2 of paper [3]).

The deviations between the models and the experimental values can be accounted for in a number of ways. The discrepancy with the MSIS-83 model below altitude 83 km could be explained by the presence of negative ions, with the values of negative ion to electron concentration ratio ranging from 0.2 at 82 km to 0.5 at 76 km. Also a positive ion mass smaller than the assumed one can explain the discrepancy, indicating for example hydrated protons with a mean hydration index slightly greater than one. The discrepancy with the CIRA model above 88 km could be due to temperatures of the order 30–40 % less than in the model. All these are realistic alternatives. The suggested negative ion to electron concentrations are small. Low concentrations of negative ions may be present for the solar zenith angle of 85°. Very low temperatures may be expected around the summer mesopause at high latitudes. In general, the accuracy of the measurements is of the order of the discrepancy between the atmospheric models.

A special feature was seen at 2058–2134 UT in the same narrow altitude region that showed

signs of heavier ions. The signal was weaker elsewhere, but around the altitude 86 km there was a 2 km thick layer with exceptionally large coherence times. These are shown in figure 7 of paper [3]. To explain this feature by local temperature variations is not reasonable, since temperature of only 40 K would be required. A possible explanation is a layer of very massive ions. These could be hydrated protons with the hydration index of the order of 10. Such ions have been measured by rocket experiments in the arctic summer mesosphere in the presence of noctilucent clouds (Kopp et al., 1985). The radar experiment itself does not allow to determine whether the time variations seen in this layer are due to true temporal variations or caused by horizontal drift of a structured layer.

As was shown by Röttger et al. (1990), there exists an alternative interpretation for this special event, in the form of the PMSE phenomenon. Collis et al. (1988) investigated this time period in more detail, but having in mind the interpretation based on ion mass variations. However, figure 1 of Collis et al. shows a clear increase of the scattered power, in addition to the spectrum narrowing, at the layer altitude. This is also seen in figure 2 of paper [3]. This feature in the data resembles closely that shown by Röttger et al. (1990) for the UHF radar during a PMSE display, which was recorded simultaneously with a 46.9 MHz VHF radar. The effect of the increase in ion mass on the incoherent scatter spectrum is demonstrated in figure 7. Figure 7 shows incoherent scatter spectra calculated from expression (1) at the altitude 85 km, corresponding to the conditions given for the time 0005 UT on 14 August 1989 in paper [6], but calculated for different mean ion masses. When the ion mass increases the spectrum narrows, but at the same time the total power in the spectrum does not change. Thus, if the limiting bandwidth of the radar receiver system is large enough, one should see no change in the incoherently scattered power due to ion mass increase. So a remarkable power increase together with the spectrum narrowing would point towards the occurence of a PMSE.

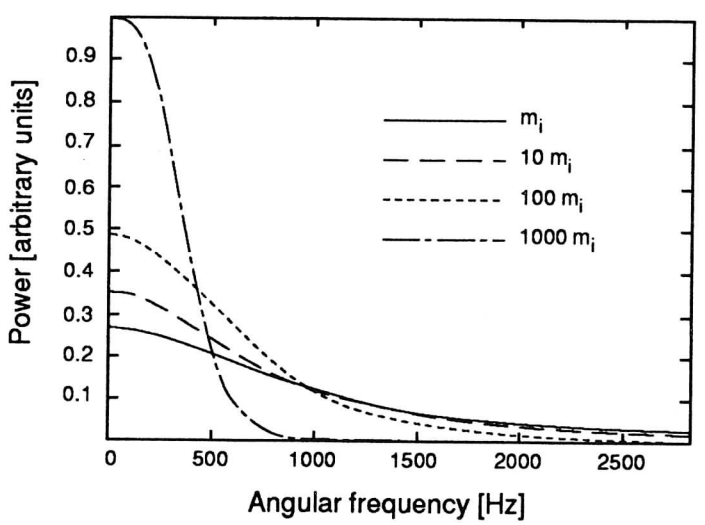


*Figure 7. The effect of the increase in ion mass on the incoherent scatter spectrum, calculated from expression (1) for the conditions given in paper [6] at 0005 UT on 14 August 1989, at the altitude 85 km.*

Although the theories behind the PMSE are many and none of them is generally accepted as the one which produces all the features related to the PMSE, it could be mentioned that the mechanism proposed by Kelley et al. (1987) is based on the existence of heavy ions in the mesopause region. It thus appears that a quantitative estimate of ion mass in the layer may not be possible due to the PMSE, but even the presence of the PMSE might qualitatively support the existence of a layer with heavier ions.

A better alternative to assumptions and model variables in interpreting incoherent scatter spectral widths as physical parameters, is to use exact measurements. This is done in paper [4] where temperature measurements by a $Na$ lidar experiment are used. The calculated spectral widths in general proved to deviate from the measured ones, specially at the higher altitudes. The measured values were sometimes narrower up to a factor of three. Once the temperature is fixed, the discrepancy can be attributed to ion mass, ion neutral collision frequency or electron to ion temperature ratio. The extreme ion mass profiles however usually have a pronounced limiting edge, which should appear also in the spectral width profile. Such a feature is not seen in data. If electron temperature increase is supposed to explain the observations, the ratio of the temperatures would have to be greater than five, which is not a very realistic value.

One might ask if these observations are a special property of the GEN-11 experiment, or a result of of the extraordinary high ionisation due to the proton event. In order to check this, the experimental spectral widths published in literature were compared with the calculated ones using the CIRA 88 model temperature and neutral density values and assuming the ion mass to be constant. This comparison included data presented by Harper (1978), Ganguly (1980,1985), Fukuyama (1981), Ganguly and Coco (1987), Kofman et al. (1984), Hall et al. (1987, 1988), Hoppe and Hansen (1988), Turunen et al. in paper [3] and Pollari et al. in paper [2]. Figure 8 in paper [4] shows the ratio of measured to calculated spectral width. The data points are scattered, but clearly there is a tendency for the measured widths to be lower than the calculated ones. The ion-neutral collision frequency by Hill and Bowhill (1977) assumes that the collision cross section is inversely proportional to the relative velocity. This makes the collision frequency depend only on neutral density, masses, percentages of neutral atmospheric molecules and atoms and on their polarizabilities. If the adopted ion-neutral collision frequency is incorrect, this could be due to a more sophisticated interaction process or imprecise values of the molecular and atomic polarizabilities.

One should note that in paper [4] the use of expressions (2) and (4) corresponds to an intrinsically decoupled use of expressions (3) and (4). The effect of negative ions on scattered power was not taken into account. This contrasts with the method of paper [6] where expressions (3) and (4) are solved for physical parameters at the lower altitudes in a consistent way.

The use of EISCAT incoherent scatter data as constraints for ion chemical models in paper [5] resulted in nitric oxide concentrations, which were typical for geophysically disturbed times. Peak concentrations just less than $2 \cdot 10^9 \mathrm{cm}^{-3}$ occur at 100 km, corresponding to the active and disturbed profiles of Grossmann et al. (1985). The modelling effort, however, was done by carefully selecting observations which represented quiet conditions.

McEwan and Phillips (1975) estimate that the mean life time of nitric oxide in the mesosphere is about 3.7 days with respect to vertical transport. Life time with respect to chemical loss processes is about 8 days. Thus transport is the dominant factor controlling the concentration of nitric oxide.

At high latitudes, energetic particle precipitation into the thermosphere during auroral activity can enhance the nitric oxide concentration. The observations with the UHF radar did in fact include periods of auroral activity in the post-midnight (Burns et al., 1990) and morning sectors (Hargreaves and Devlin, 1990). The enhancement of the nitric oxide concentration could be due to an increased production of thermospheric $N(^2D)$ by precipitation

$$N_2 + e \rightarrow N(^2D) + N(^4S) + e$$

in addition to

$$NO^+ + e \rightarrow N(^2D) + O$$

and

$$N_2^+ + O \rightarrow N(^2D) + NO^+$$

followed by

$$N(^2D) + O_2 \rightarrow NO + O \quad ,$$

and then transport into the mesosphere. The resulting enhancement of mesospheric $NO$ coupled with its long lifetime could be responsible for high concentrations in the D-region. Under quiet daytime conditions this situation might persist for hours.

Figure 8 in paper [6] shows the results of interpreting the EISCAT measurements at 0005 and 0255 UT on 14 August 1989, via the solution of the SIC-model. The raw electron densities from expression (2) are also shown in figure 8a of paper [6]. The negative ions have a considerable effect on the electron density profile at 0005 UT, whereas during the daytime only the Debye-length correction is seen to be effective. The value of this correction is of the order of 5–10 %. The mean ion masses in figure 8c of paper [6] are similar for the two times, except for the region of negative ions. In addition, the overall forms of the ion mass profiles are similar to the profile adopted in paper [4] (see figure 3 in paper [4]). The deduced temperature profiles, shown in figure 8d, resemble each other closely for the two selected times. The differences are of the order of 5-15 K and correspond to the small differences in ion masses at the altitudes of no negative ions. The negative ion profiles resulting from the SIC-model are shown as solid lines in figure 8b of paper [6]. At midnight, the concentrations of negative ions and electron are equal at the altitude of 75 km. The negative ion to electron concentration ratio $\lambda$ is 8 at the height of 70 km. At daytime, a sign of negative ions appears only in the lowest measured gate at 70 km, the value of $\lambda$ being less than 1. As a consistency check of the model and the radar data, $\lambda$ profiles from the solution of expressions (3) and (4) are plotted in figure 8d as dashed lines. The different $\lambda$ profiles do not quite agree but they are consistent to within an accuracy better than 25 %.This is the difference between the night-time value derived from expressions (3) and (4) and the SIC-model value at 70 km.

Selected altitude profiles of ion concentrations are plotted in figure 9 of paper [6]. The dominant positive ions are $NO^+$ and $O_2^+$, competing at different altitudes. The cluster ions are not strikingly abundant compared to a normal D-region situation, where primary ion production rates are much less than in our case of a solar proton event. At altitudes higher than the actual negative ion region the dominant negative ion is $O_2^-$. At night-time this is replaced by the dominance of $CO_3^-$ and $NO_3^-$ below 75 km. At day-time, $HCO_3^-$ also sets in at 70 km.

The electron density values are checked against cosmic radio noise absorption measurements in figure 10 of paper [6]. Although the altitude range of EISCAT measurement is limited, the comparison

can be made during night-time, when free electrons are lost due to electron attachment to neutrals at low altitudes. The deduced electron density is seen to be more consistent with the riometer data than the raw density.

A contour plot of negative ion to electron concentration ratio as a function of time and altitude is given in figure 12 of paper [6]. The three nights show similar behaviour. Negative ions start to appear at the height of 78 km, and in significant amounts below 75 km. A small difference is seen in the first night. This might be a sign of the neutral atmosphere response to the solar proton event, because figures 10 and 12 in paper [6] were formed using average profiles from figure 8 of paper [6].

Most confidence in the validity of the incoherent scatter data interpretation in paper [6] results from a comparison of the deduced temperatures with those measured by the *Na* lidar experiment. The measured temperatures were given as average profiles in paper [4]. This comparison is shown in figure 8.

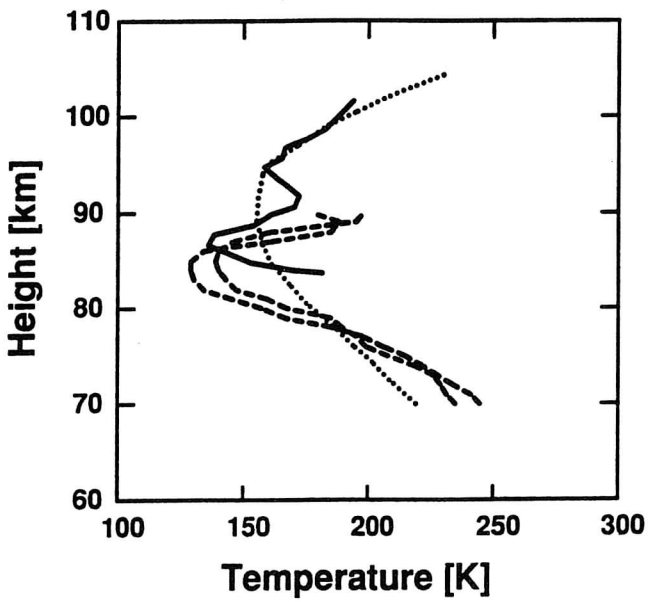


*Figure 8. Comparison of the deduced temperature profiles (dashed lines) at 0005 and 0255 Ut on 14 August 1989 with an average profile (solid line) from lidar measurements at Andøya during the night 14–15 August 1989 (from paper [4]). The extrapolated MSIS86 model temperature used as initial values in calculations is also shown (dotted line).*

The temperature minimum measured by the lidar experiment is not exactly given by the MSIS86 model temperature, although the height averaged temperature in this region is quite close. The deduced mesopause temperatures instead closely match the lidar temperature average. Also the sharp gradient above mesopause is present in the deduced temperatures. The gradients around mesopause even match those of the lidar temperature average. A clear difference between the deduced temperatures and the lidar temperature average is in the mesopause altitude, which is 85 and 87 km for the deduced and lidar temperatures, respectively.

# 6. CONCLUSIONS

The EISCAT UHF and VHF radars are powerful tools for investigating D-region aeronomy, provided that a sophisticated analysis procedure is used both in handling the raw radar data and in interpreting it as physical parameters.

Receiver recovery effects can be reduced if spectral information is present in radar data. The range ambiguous zero lag of a multipulse experiment can be used to improve statistical accuracy of the data in practical applications. The range ambiguities produced by the special modulation structure of a Barker-coded pulse to pulse correlation D-region experiment can be removed from data. Without this correction electron densities are usually underestimated, correlation times can be erroneous by 20 % or more in the worst case, and a considerable error on parameters derived from spectral width is caused. The ion velocities are not affected by the correction. A case study with the EISCAT VHF radar on 27 April 1987 showed that at the altitude of 70 km the negative ion to electron concentration ratio would be 30 % too high, if it were estimated without the correction.

The description of incoherent scatter at D-region altitudes by Fukuyama and Kofman (1980) is in excellent agreement with the description of incoherent scatter based on the work by Dougherty and Farley (1960, 1963) and Swartz and Farley (1979). Once accepted, the resulting analytically simple form can be used to infer one of the parameters mean ion mass, ion-neutral collision frequency, temperature and negative ion to electron concentration ratio, if the others are fixed by independent measurements or model values. If one wants to make no other a priori assumptions on the behaviour of the atmosphere, a detailed ion chemistry model of the D-region can be used to establish relations which allow the determination of more than one physical parameter from the spectral width of the incoherently scattered signal.

However, there is a possible conflict of the presently accepted incoherent scatter theory with experimental data. The measured spectral widths in D-region appear to be narrower than those calculated from expression (4), using assumptions on ion mass and a model neutral atmosphere, together with the description of ion-neutral collision frequency for momentum transfer as given by Hill and Bowhill (1977). There has been a controversy as to the introduction of the collisional term in the incoherent scatter theory. Dougherty and Farley used a particle conserving relaxation term. Waldteufel (1965, 1969, 1970) formulated different collision terms allowing for momentum conservation and temperature changes during collisions. Grassmann (1988) also considers modification of the collision term to conserve density, momentum and energy. As Waldteufel's and Grassmann's formulations will yield even wider spectra than that of Dougherty's and Farley's, it is natural to use the description adopted here. Ganguly and Coco (1987) also found that the formulation by Dougherty and Farley fits the experimental results best. They note that during collisions ions lose both momentum and energy to neutrals, and so far as ion gas is concerned, neither should be conserved. If the formulation by Dougherty and Farley is accepted, one concludes that in paper [4] either the collision frequency by Hill and Bowhill (1977), information about atomic and molecular polarizabilities or the improper treatment of Debye length effects causes the observed discrepancy. Possible electron gas heating by the probing radar pulses should also be considered quantitatively.

The measured altitude profiles of electron density account satisfactorily for the cosmic radio noise absorption measured by riometers. One should note that precise comparisons of this kind are difficult. First, a spatially structured precipitation region may be seen differently by the narrow beam of the EISCAT antennas compared with a standard wide beam riometer antenna. Second, the calculation of absorption from electron density profiles needs independent information about electron-neutral collision frequency, which usually is available only through models or non-simultaneous reference measurements. Third, the altitude region of EISCAT measurements is usually limited from below, whereas the whole lower ionosphere is contributing to the integrating riometer measurement.

The effective recombination rate coefficients determined on 16 February 1984 are generally consistent with previous estimates. They show a gradual decrease during the day indicating a progressive change in D-region photochemistry. The gradual change of the effective recombination coefficient between altitudes from 90 km to 75 km is consistent with a transition from molecular to hydrated ions.

Changes in electron density at the altitude region of 80–110 km as a function of solar zenith angle can be predicted by ion-chemical models, once a calibration to EISCAT measurements at a fixed zenith angle is done. Determination of neutral nitric oxide concentrations on 23 August 1985 and 14 August 1988 showed concentrations which are typically observed at geomagnetically disturbed times. The estimates based on two independent ion chemical models were consistent. Peak concentrations occurred at altitude 100 km and were just less than $2 \cdot 10^9 \mathrm{cm}^{-3}$. These high concentrations could be explained by enhancement of thermospheric $NO$ concentration by energetic particle precipitation in the morning sector, followed by transport into the D- and lower E-region, where concentrations may persist due to the long lifetime of $NO$.

Under suitable conditions, even in the D-region, the EISCAT UHF radar is capable of providing spectral information on the incoherently scattered signal. Doppler velocities are clearly measurable and can be used for studies of mesospheric dynamics. If spectral data is integrated over time, the effect of atmospheric waves must be taken into account by correcting the spectra individually for the Doppler shift. The obtained ion-neutral collision frequencies are reliable within the accuracy of the available neutral atmosphere models. If the incoherent scatter signal is assumed to be uncontaminated by the polar mesosphere summer echoes, a more or less persistent layer of heavy ions was observed on 1 July 1985 at altitude 86 km. These ions are possibly of type $H^+(H_2O)_n$, with a mean value of n around 2, but during short intervals around up to 10. This conclusion is consistent with measurements in the vicinity of a structured noctilucent cloud. However, the quantitative estimate of the very high ion mass should be treated with some caution, due to the possible occurence of the PMSE phenomenon.

The electron density, the mean ion mass, the negative ion to electron concentration ratio and the neutral temperature estimated from EISCAT measurements on 13–14 August 1989 during a solar proton event, were in agreement with all other information available for comparison. The estimation was based on the use of a detailed ion chemistry model, which includes chemical reactions between 35 different ions. A selected neutral atmosphere model was used to provide initial values of temperature and fixed proportions for concentrations of the neutral constituents. Satellite data on proton flux in the solar wind was used to calculate ion production at D-region altitudes. The concentrations of the cluster ions were not dominating even at the lowest altitudes down to 70 km during the high ionisation produced by the protons. Nevertheless, higher mean ion masses, approaching the value 50, were seen at the altitude of mesopause during the day and twilight conditions, and at 70 km during the twilight

conditions. At mesopause the dominating ion was $O_2^+$, at other altitudes it was $NO^+$. In day-time the dominant negative ion was $O_2^-$ and at the lowest altitudes $HCO_3^-$. At twilight $O_2^-$ was replaced by $CO_3^-$ and $NO_3^-$ below altitude of 75 km.

If the adopted description of incoherent scatter at D-region altitudes can be accepted, a vast number of applications will benefit from the use of interpretations similar to that of paper [6]. For example it would be straightforward to reveal the possible effect of the solar proton event on neutral atmosphere. Instead of adjusting the temperature as in paper [6], the temperature could be fixed to the values from a simultaneous *Na* lidar experiment. Concentrations of the neutral minor constituents could then be estimated via the application of the ion chemistry model.

When more accurate neutral atmosphere models become available, the interpretation presented in paper [6] can be developed to give a routine analysis of EISCAT incoherent scatter data from D-region. It is also possible to include the estimation of the precipitating electron spectrum as one of the parameters to be deduced routinely from incoherent scatter data. Usually one applies a fixed effective recombination rate coefficient in these estimations. This is, however, a crude approximation of the D-region, and can be avoided by the use of an ion chemistry model. Also, if the electron spectrum is parametrized in some simple form, other parameters of aeronomical interest will still remain available.

## REFERENCES:


Alcaydé, D., (1981),
An analytical static model of temperature and composition from 20 to 2000 km altitude. *Ann. Geophys. 37, 515.*

Armistead, G.W., J.V. Evans and W.A. Reid, (1972),
Measurements of D- and E-region electron densities by the incoherent scatter technique at Millstone Hill. *Radio Sci. 7, 153.*

Burns, C.J., W.G. Howarth and J.K. Hargreaves, (1990),
High-resolution incoherent scatter radar measurements during electron precipitation events. *J. Atmos. Terr. Phys. 52, 205.*

Chakrabarty, D.K., P. Chakrabarty and G. Witt, (1978),
An attempt to identify the obscured paths of water cluster ions build–up in the D–region. *J. Atmos. Terr. Phys. 40, 437.*

CIRA, (1972),
COSPAR International Reference Atmosphere, Akademie-Verlag, Berlin.

Collis, P.N. and J. Röttger, (1990),
Mesospheric studies using the EISCAT UHF and VHF radars: a review of principles and experimental results. *J. Atmos. Terr. Phys. 52, 569.*

Collis, P.N., T. Turunen and E. Turunen, (1988),
Evidence of heavy positive ions at the summer arctic mesopause from the EISCAT UHF incoherent scatter radar. *Geophys. Res. Lett. 15, 148.*

Dougherty, J.P. and D.T. Farley, (1960),
A theory of incoherent scattering of radio waves by a plasma. *Proc. Roy. Sci. Ser. A, 259, 79.*

Dougherty, J.P. and D.T. Farley, (1963),
A theory of incoherent scattering of radio waves by a plasma, 3, Scattering in a partly ionized gas. *J. Geophys. Res. 68, 5473.*

Fleming, E.L., S. Chandra, M.R. Shoeberl and J.J. Barnett, (1988),
Monthly mean global climatology of temperature, wind, geopotential height, and pressure for 0-120 km. *NASA Tech. Mem., 100697.*

Folkestad, K., T. Hagfors and S. Westerlund, (1983),
EISCAT: an updated description of technical characteristics and operational capabilities. *Radio Sci. 18, 867.*

Fukuyama, K., (1981),
Incoherent Scatter Radar Observations of Wavelike Structures in the Mesosphere Over Arecibo. *J. Geophys. Res. 86, 9152.*

Fukuyama, K. and W. Kofman, (1980),

Incoherent scattering of an electromagnetic wave in the mesosphere: a theoretical consideration. *J. Geomagn. Geoelect. 32, 67-81.*

Fukuyama, K., Y. Maekawa, S. Fukao and S. Kato, (1987),

Ionospheric D-region temperatures, and electron and neutral densities observed by the incoherent scatter technique at Arecibo. *Annales Geophys. 5A, 289.*

Ganguly, S., (1980),

Incoherent scatter observations of mesospheric dynamics at Arecibo. *Geophys. Res. Lett. 7, 369.*

Ganguly, S., (1985),

The sunrise and sunset transitions in the mesosphere. *J. Atmos. Terr. Phys. 47, 643.*

Ganguly, S. and D. Coco, (1987),

Incoherent scattering from the collision dominated D-region. Comparison of theories with experimental data. *J. Atmos. Terr. Phys. 49, 549.*

Grassmann, V., (1988)

Inkohärente Streuung von Radiowellen durch ein Plasma unter Berücksichtigung von Teilchen-Stößen *Report MPAE-W-100-88-07*, Max Planck Institut für Aeronomie, Katlenburg-Lindau.

Grossmann, K.U., W.G. Frings, D. Offermann, L. Andre, E. Kopp and D. Krankowsky, (1985),

Concentrations of $H_2O$ and $NO$ in the mesosphere and the lower thermosphere at high latitudes. *J. Atmos. Terr. Phys. 47, 291.*

Hall, C., (1988),

Recent D-region research using incoherent scatter radar. *Adv. Space Res. 9, (5)163.*

Hall, C.M. and A. Brekke, (1988),

High Schmidt Numbers in the Mesopause Region from 224 MHz Incoherent Backscatter. *Geophys. Res. Lett. 15, 561.*

Hall, C.M., T. Devlin, A. Brekke and J.K. Hargreaves, (1988),

Negative ion to electron number density ratios from EISCAT mesospheric spectra. *Physica Scripta 37, 413.*

Hall, C.M., U.-P. Hoppe, P.J.S. Williams and G.O.L. Jones, (1987),

Mesospheric measurements using the EISCAT VHF system: First results and their interpretation. *Geophys. Res. Lett. 14, 1187.*

Hargreaves, J.K., H.J.A. Chivers and S. Nielsen, (1979),

Properties of Spike Events in Auroral Radio Absorption. *J. Geophys. Res. 84, 4245.*

Hargreaves, J.K and T. Devlin, (1990),

Morning sector electron precipitation events observed by incoherent scatter radar. *J. Atmos. Terr. Phys 52, 193.*

Harper, R.M., (1978),

Preliminary measurements of the ion component of the incoherent scatter spectrum in the 60-90 km region over Arecibo. *Geophys. Res. Lett., 5, 784.*

Heaps, M.G., (1978),

Parametrization of the cosmic ray ion-pair production rate above 18 km. *Planet. Space Sci. 26, 513.*

Hedin, A.E., (1983),

A revised thermospheric model based on mass spectrometer and incoherent scatter data: MSIS-83. *J. Geophys. Res. 88, 10170.*

Hedin, A.E., (1987),

MSIS–86 Thermospheric Model. *J. Geophys. Res. 92, 4649.*

Heroux, L. and H.E. Hinteregger, (1978),

Aeronomical Reference Spectrum for Solar UV below 2000Å. *J. Geophys. Res. 83, 5305.*

Hill, R.J. and S.A. Bowhill, (1977),

Collision frequencies for use in the continuum momentum equations applied to the lower ionosphere. *J. Atmos. Terr. Phys. 39, 803.*

Hoppe, U.-P., C. Hall and J. Röttger, (1988),

First observations of summer polar mesospheric backscatter with a 224 MHz radar. *Geophys. Res. Lett. 15, 28.*

Hoppe, U.-P. and T.L. Hansen, (1988),

Studies of vertical motions in the upper mesosphere using the EISCAT UHF radar. *Ann. Geophys. 6, 181.*

Huffman, R.E., D.E. Paulsen, J.C. Larabee and R.B. Cairns, (1971),

Decrease in D-region $O_2(_1\Delta^g)$ photo–ionization rates resulting from $CO_2$ absorption. *J. Geophys. Res. 76, 1028.*

Huuskonen, A., P. Pollari, T. Nygren and M.S. Lehtinen, (1988),

Range ambiguity effects in Barker–coded multipulse experiments with incoherent scatter radars. *J. Atmos. Terr. Phys. 50, 265-276.*

Johannessen, A. and E.V. Thrane, (1974),

Rocket study of the high-latitude summer mesopause. *Indian J. Radio Space Phys. 3, 128.*

Jones, A.V., (1974),

Aurora, D. Reidel Publishing Company, Dordrecht, Holland.

Kane, J.A., (1961),

Re–evaluation of ionospheric electron densities and collision frequencies derived from rocket measurements of refractive index and attenuation. *J. Atmos. Terr. Phys. 23, 338.*

Kelley, M.C., T.D. Farley and J. Röttger, (1987),

The effect of cluster ions on anomalous VHF backscatter from the summer polar mesosphere. *Geophys. Res. Lett. 14, 1031.*

Kofman, W., F. Bertin, J. Röttger, A. Cremieux and P.J.S. Williams, (1984),

The EISCAT mesospheric measurements during the CAMP campaign. *J. Atmos. Terr. Phys. 46, 565.*

Kopp, E., P. Eberhardt, U. Herrmann and L.G. Björn, (1985),

Positive ion composition of the high-latitude summer D-region with noctilucent clouds. *J. Geophys. Res. 90, 13041.*

La Hoz, C., J. Röttger, M. Rietveld, G. Wannberg and S.J. Franke, (1989),

The status and planned developments of EISCAT in mesosphere and D-region experiments. *Handbook for MAP 28, 476.*

LaLonde, L.M., (1966),

Incoherent Backscatter Observations of Sporadic E. *J. Geophys. Res. 71, 5059.*

Lean, J.L. and A. Skumanich, (1983),

Variability of the Lyman Alpha Flux with Solar Activity. *J. Geophys. Res. 88, 5751.*

Lehtinen, M.S., (1986),

Statistical Theory of Incoherent Scatter Radar Measurements. *EISCAT technical note 86/45*, EISCAT Scientific Association, Kiruna.

Lehtinen, M. and A. Huuskonen, (1986),

The use of multipulse zero lag data to improve incoherent scatter radar power profile accuracy. *J. Atmos. Terr. Phys. 48, 787.*

Mathews, J.D., (1976),

Measurements of the diurnal tides in the 80- to 100-km altitude range at Arecibo. *J. Geophys. Res. 81, 4671.*

Mathews, J.D., (1978),

The effect of negative ions on collision–dominated Thomson scattering. *J. Geophys. Res. 83, 505.*

Mathews, J.D., (1981),

D–region research at Arecibo. *J. Atmos. Terr. Phys. 43, 549.*

Mathews, J.D., (1984),

The incoherent scatter radar as a tool for studying the ionospheric D-region. *J. Atmos. Terr. Phys. 46, 975.*

Mathews, J.D., J.K. Breakall and S. Ganguly, (1982),
The measurement of diurnal variations of electron concentration in the 60-100 km ionosphere at Arecibo. *J. Atmos. Terr. Phys. 44, 441.*

McEwan, M.J., and L.F. Phillips, (1975),
Chemistry of the atmosphere, Edward Arnold Ltd., London.

Meira, L. G., (1971),
Rocket Measurements of Upper Atmospheric Nitric Oxide and Their Consequences to the Lower Ionosphere. *J. Geophys. Res. 76, 202.*

Mitra, A.P. and J.N. Rowe, (1972),
Ionospheric effects of solar flares–VI. Changes in D–region ion chemistry during solar flares. *J. Atmos. Terr. Phys. 34, 795.*

Ohshio, M., R. Maeda, H. Sakagami, (1966),
Height distribution of local photoionization efficiency. *J. Radio Res. Lab. 13, 245.*

Press, W.H., B.P. Flannery, S.A. Teukolsky, W.T. Vetterling, (1986),
Numerical Recipes, The Art of Scientific Computing, Cambridge University Press, New York, USA.

Rastogi, P.K. and R.F. Woodman, (1974),
Mesospheric studies using the Jicamarca incoherent-scatter radar. *J. Atmos. Terr. Phys. 36, 1217.*

Reagan, J.B. and T.M. Watt, (1976),
Simultaneous satellite and radar studies of the D-region ionosphere during the intense solar particle events of August 1972. *J. Geophys. Res. 81, 4579.*

Rees, M.H., (1963),
Auroral Ionization and Excitation by Incident Energetic Electrons. *Planet. Space Sci. 11, 1209.*

Rees, M.H., (1989),
Physics and Chemistry of the upper Atmosphere, Cambridge, Great Britain.

Risbeth, H., A.P. van Eyken, B.S. Lanchester, T. Turunen, J. Röttger, C. Hall and U.-P. Hoppe, (1988),
EISCAT VHF radar observations of periodic mesopause echoes. *Planet. Space Sci. 36, 423.*

Röttger, J., C. La Hoz, M.C. Kelley, U.-P. Hoppe and C. Hall, (1988)
The structure and dynamics of polar mesosphere summer echoes observed with the EISCAT 224 MHz radar. *Geophys. Res. Lett. 15, 1353.*

Röttger, J., M.T. Rietveld, C. La Hoz, T. Hall, M.C. Kelley and W.E. Swartz, (1990),

Polar mesosphere summer echoes observed with the EISCAT 933-MHz radar and the CUPRI 46.9-MHz radar, their similarity to 224-MHz radar echoes, and their relation to turbulence and electron density profiles. *Radio Sci. 25, 671.*

Schlegel, K., (1979),

*Report MPAE–W–05–79–01*, Max–Planck–Institut für Aeronomie, Katlenburg–Lindau

Sechrist, Jr., C.F., (1974),

Comparisons of techniques for measurement of D-region electron densities. *Radio Sci. 9, 137.*

Swartz, W.E. and D.T. Farley, (1979),

A theory of incoherent scattering of radio waves by a plasma, 5, The use of the Nyquist theorem in general quasi–equilibrium situations. *J. Geophys. Res. 84, 1930.*

Swider, W. and R.S. Narcisi, (1975),

A study of the nighttime D region during a PCA event. *J. Geophys. Res. 80, 655.*

Tanenbaum, B.S., (1968),

Continuum theory of Thomson scattering. *Phys. Rev. 171, 215.*

Taylor, G.N., (1975),

Incoherent scatter measurements of E- and upper D-region ionization during three solar flares. *J. Atmos. Terr. Phys. 37, 349.*

Tepley, C.A. and J.D. Mathews, (1978),

Preliminary measurements of ion–neutral collision frequencies and mean temperatures in the Arecibo 80- to 100-km altitude region. *J. Geophys. Res. 83, 3299.*

Thomas, L. and M.R. Bowman, (1985),

Model studies of the D–region negative–ion composition during day–time and night–time. *J. Atmos. Terr. Phys. 47, 547.*

Torkar, K.M. and M. Friedrich, (1983),

Tests of an ion–chemical model of the D– and lower E–region. *J. Atmos. Terr. Phys. 45, 369.*

Torr, M.R., D.G. Torr, R.A. Ong and H.E. Hinteregger, (1979),

Ionization frequencies for major thermospheric constituents as a function of solar cycle 21. *Geophys. Res. Lett. 6, 771.*

Turunen, E. , C. Hall and T. Turunen, (1987),

Future developments of auroral D-region research using the EISCAT VHF incoherent scatter radar. *Proceedings of the* 8th *ESA symposium on European Rocket and Balloon Programmes and Related Research, Sunne, Sweden, ESA SP-270, 461.*

Turunen, E. , H. Matveinen and H. Ranta, (1992),

Sodankylä Ion Chemistry (SIC) Model. *Sodankylä Geophysical Observatory Report No. 49*, Sodankylä, Finland.

Turunen, T., (1986),

GEN–system—A new experimental philosophy for EISCAT radars. *J. Atmos. Terr. Phys. 48, 777.*

Turunen, T. and J. Silén, (1984),

Modulation patterns for the EISCAT incoherent scatter radar. *J. Atmos. Terr. Phys. 46, 593.*

Vallinkoski, M., (1988),

Statistic of incoherent scatter multiparameter fits. *J. Atmos. Terr. Phys. 50, 839.*

Waldteufel, P., (1965),

Introduction de l'effet des collisions élastiques dans l'équation de Boltzmann d'un gaz faiblement ionisé application a la diffusion incohérente d'une onde électromagnétique par l'ionosphére. *Annales Geophys. 21, 106.*

Waldteufel, P., (1969),

Valeur et variation diurne de la densité atmosphérique á 100 km d'altitude. *Planet. Space Sci. 17, 725.*

Waldteufel, P., (1970),

A study of seasonal changes in the lower thermosphere and their implications. *Planet. Space Sci. 18, 741.*

Wisemberg, J. and G. Kockarts, (1980),

Negative Ion Chemistry in the Terrestrial D Region and Signal Flow Graph Theory. *J. Geophys. Res. 85, 4642.*